National Library
of Canada

Acquisitions and
Bibliographic Services Branch

395 Wellington Street
Ottawa, Ontario
K1A 0N4

Bibliothèque nationale
du Canada

Direction des acquisitions et
des services bibliographiques

395, rue Wellington
Ottawa (Ontario)
K1A 0N4

Your file Votre reference

Our file Notre reference

NOTICE

The quality of this microform is heavily dependent upon the quality of the original thesis submitted for microfilming. Every effort has been made to ensure the highest quality of reproduction possible.

If pages are missing, contact the university which granted the degree.

Some pages may have indistinct print especially if the original pages were typed with a poor typewriter ribbon or if the university sent us an inferior photocopy.

AVIS

La qualité de cette microforme dépend grandement de la qualité de la thèse soumise au microfilmage. Nous avons tout fait pour assurer une qualité supérieure de reproduction.

S'il manque des pages, veuillez communiquer avec l'université qui a conféré le grade.

La qualité d'impression de certaines pages peut laisser à désirer, surtout si les pages originales ont été dactylographiées à l'aide d'un ruban usé ou si l'université nous a fait parvenir une photocopie de qualité inférieure.

Canada

Theoretical Study of Three Problems Related to the Electrophoresis of Polyelectrolytes

by

Sylvain Hubert

A thesis presented to the University of Ottawa in fulfilment of the thesis requirement for the degree of Master of Science in Physics

Ottawa, Ontario, 1995

ISBN 0-612-07821-3

Canada

UNIVERSITÉ D'OTTAWA
UNIVERSITY OF OTTAWA

Acknowledgments

I would like to give special thanks to my supervisor, Dr. Gary Slater, for introducing me to the physics of polymers in the summer of 1993. Since then, his intuition in physics as well as his sense of humor during the course of my research have impressed me. His guidance and his understanding have always been a great source of inspiration. I also appreciate the great amount of time he spent helping me with corrections.

I would like to give my sincere gratitude to Dr. Ivan L'Heureux, for helping me understand Stochastic Processes and for taking the time to polish the English in this thesis. Thanks to Dr. Charles R. Doering (Clarkson University) for early calculations on the stochastic mechanics of reptation with energy fluctuations. I would also like to thank Dr. Jean-Louis Viovy for his contribution to the work on the DNA separation process in ultra-dilute polymer solutions.

Thanks to my family: Pauline Séguin Hubert (my mother), Jean-Claude Hubert (my father), Manon and Chantal (my sisters), and Mario and Stéphane (my brothers) for always believing in me and giving me their support. I would also like to thank Pierre Robert for his friendship and all those enjoyable nights on the computer. Thanks to my great friends and colleagues at work: Grant I. Nixon, Hong Guo, Claude Desruisseaux, Saeed Hadjifaradji, Steve Guillouzic, Song Yan Wu, and Robert Parent for their friendship, their delightful discussions, and, most of all, for making the university life fun. Thanks to my close friends Fabrice Rappold, Céline Paquet, Vincent Allain, Julie Chouiri, and Mireille McGregor for always being there when I need them. They have been very much appreciated throughout the years. Thanks for all those joyful nights out. I also thank FCAR and the University of Ottawa for their scholarships and for offering me a chance to pursue my studies in polymer physics.

Finally, I would like to give my deepest thanks to my dearest friend Ros Salvador for her endless support, patience, and enduring love.

Summary

The Human Genome Initiative is a worldwide research effort whose goals are to analyze the detailed nature of human DNA and determine the chemical composition of all human genes. This project is expected to immensely benefit medical science. It will help us understand and eventually treat many of the hundreds of genetic diseases that afflict mankind, as well as the many multifactorial diseases in which genetic predisposition plays an important role. In the last 30 to 40 years, the technology has advanced to a stage of development at which such a project can realistically be contemplated. Although mapping of human genes began early in the 20th century, about 99% of the genome is still unknown. Therefore, the development of new separation processes as well as a better understanding of the old separation techniques are needed to achieve the goals of this project.

In 1994, P. Mayer, G.W. Slater and G. Drouin studied mathematically a new approach for the separation of DNA in free solutions where one attaches a neutral globular object at the end of the DNA molecule. This object would increase the friction and slow down the smaller DNA molecules more than the larger ones. In Chapter 2, we propose to attach a neutral flexible polymer instead. We demonstrate that this has the advantage of being more efficient as a friction generator.

In 1994, A.E. Barron, H.W. Blanch and D.S. Soane obtained good DNA separations in ultra-dilute polymeric solutions. In Chapter 3, we develop the first theoretical model of this promising technology. This model is based on polymer hydrodynamics, molecular collisions and drag forces.

In 1993, Zimm and Lumpkin proposed a new reptation model to explain gel electrophoresis of polyelectrolytes in irregular matrices. Following this work, we propose in Chapter 4 a more detailed model of this problem where the well-known memory effects of the standard reptation theory are taken into account. Our results are in qualitative agreement with available experimental results.

Cette ouvrage est dédié à la douce mémoire de ma chère et tendre mère pour qui mon amour n'aura jamais de frontières. Elle sera toujous présente dans nos coeurs. Tu nous manques beaucoup!

Table of Contents

Chapitre 1

Introduction

1.1 Introduction

C'est en 1953 que le célèbre modèle de la double hélice de l'ADN a été proposé par Watson et Crick [1] grâce aux résultats expérimentaux obtenus par Wilkins et Randall [2], et Franklin [3]. Cette molécule chargée que l'on retrouve en 46 exemplaires (les chromosomes) dans toutes les cellules du corps humain, contient plus de 3 x 10^9 paires de nucléotides (bp) d'ADN [4] (ce qui équivaut approximativement à 750 mégaoctets d'information). Il existe quatre différents types de nucléotides (appelés bases) dans l'ADN: G (guanine), A(adénine), T (thymine) et C (cytosine). C'est l'ordre de ces bases dans la chaîne d'ADN qui nous permet de distinguer et d'identifier les différentes protéines d'un organisme. La connaissance de ce code génétique donnerait aux biologistes, médecins, chimistes, physiciens et autres, la possibilité de mieux comprendre le fonctionnement du corps humain et des autres organismes vivants, pouvant ainsi donner naissance à plusieurs nouveaux médicaments et traitements médicaux.

Depuis vingt ans, la connaissance du rôle que joue la molécule d'ADN dans les traits héréditaires s'est accrue considérablement. Plusieurs croyaient que l'étude de cette molécule resterait entre les mains des biologistes, mais sa complexité demande l'aide de plusieurs autres disciplines: le génie, les mathématiques, la chimie, la physique, etc... C'est en février 1988 que le projet du génome humain fut lancé au États-Unis [5]. Le but principal du projet est évidemment le séquençage de l'ADN, i.e. la détermination de la séquence exacte des nucléotides qui composent le matériel chromosomique d'un humain. Grâce à cette initiative, les protocoles expérimentaux et les instruments utilisés dans l'analyse de l'ADN se sont grandement améliorés et nous ont permis de mieux comprendre la structure et le rôle de cette macromolécule. Mais malgré les efforts fournis par les différents pays prenant maintenant part au projet, plus de 99% du génome humain nous est presque complètement inconnu. Seulement 10^6-10^7 bp de l'ADN ont pu être décodées en utilisant principalement la technique de l'électrophorèse dans un gel [6]. Par contre, la cartographie des chromosomes est essentiellement complétée grâce à l'invention de l'électrophorèse en champs pulsés sur gel d'agarose par Schwartz et Cantor en 1984 [7]. Plusieurs autres méthodes peuvent également être employées pour la séparation de l'ADN: l'électrophorèse dans

un milieu dilué [8] ($c < c^*$, ou c^* est la concentration d'enchevêtrement des polymères), ELSFE [9] ("End-Label Free Solution Electrophoresis"), l'électrophorèse dans un milieu concentré [10] ($c > c^*$), etc...

1.2 Technique de Séparation (Électrophorèse)

1.2.1 Séparation

Depuis quelques années, la recherche sur les méthodes de séparation de l'ADN s'est accélérée considérablement. Nous avons ainsi pu comprendre le fonctionnement de certains organismes biologiques grâce à la connaissance du système biologique humain, et vice-versa. Parmi les techniques de séparation connues, l'électrophorèse dans un gel est la plus employée. Cette technique ne nous a permis de décoder que les 10^7 premières bases de la chaîne d'ADN (moins de 1%). Il faudra donc développer de nouvelles méthodes de séparation afin de nous permettre de décoder le génome humain. Parmis ces nouvelles techniques de séparation, on retrouve l'électrophorèse dans un milieu ultra-dilué [8], l'électrophorèse d'un complexe ADN-polymère en solution libre [9], l'électrophorèse dans un milieu polymérique concentré [10], etc... Il existe également des méthodes non-électrophorétiques telle que la spectroscopie de masse [11], l'hybridation [12], etc..., qui restent encore quelque peu hypothétiques.

La Fig. 1.1 représente shématiquement le processus de l'électrophorèse. La figure est séparée en trois étapes: l'entrée des molécules, l'électrophorèse, et enfin la sortie des molécules. Sur le côté droit, on retrouve l'évolution de la distribution de masses des molécules que l'on veut séparer. La première étape consiste à introduire les molécules, qui sont dans une solution tampon ("buffer"), à l'intérieur du système d'électrophorèse que nous nommons "boîte noire". On observe également que les distributions de masses s'entremêlent les unes les autres (c'est ce que l'on veut séparer). La seconde étape du processus est l'électrophorèse. On utilise un champ électrique (E) constant ou pulsé, ou même un gradient de champ électrique, afin de provoquer le déplacement des molécules à l'intérieur de la "boîte noire". La vitesse instantannée de ces molécules en solution libre est directement reliée au champ électrique,

$$v = QE/\xi \qquad (1.1)$$

où Q ($\propto$ masse de la molécule) est la charge totale de la molécule et ξ est le coefficient de friction de la molécule. Certains polymères tel que l'ADN [13,14] ont un coefficient de friction directement proportionnel à leur masse. Dans ce cas, aucune séparation ne peut être obtenue et on parle du régime "free-draining". Il est alors préférable d'effectuer l'électrophorèse dans une matrice comme un gel ou un papier (comme en chomatographie) afin d'introduire la dépendance de la masse moléculaire de la

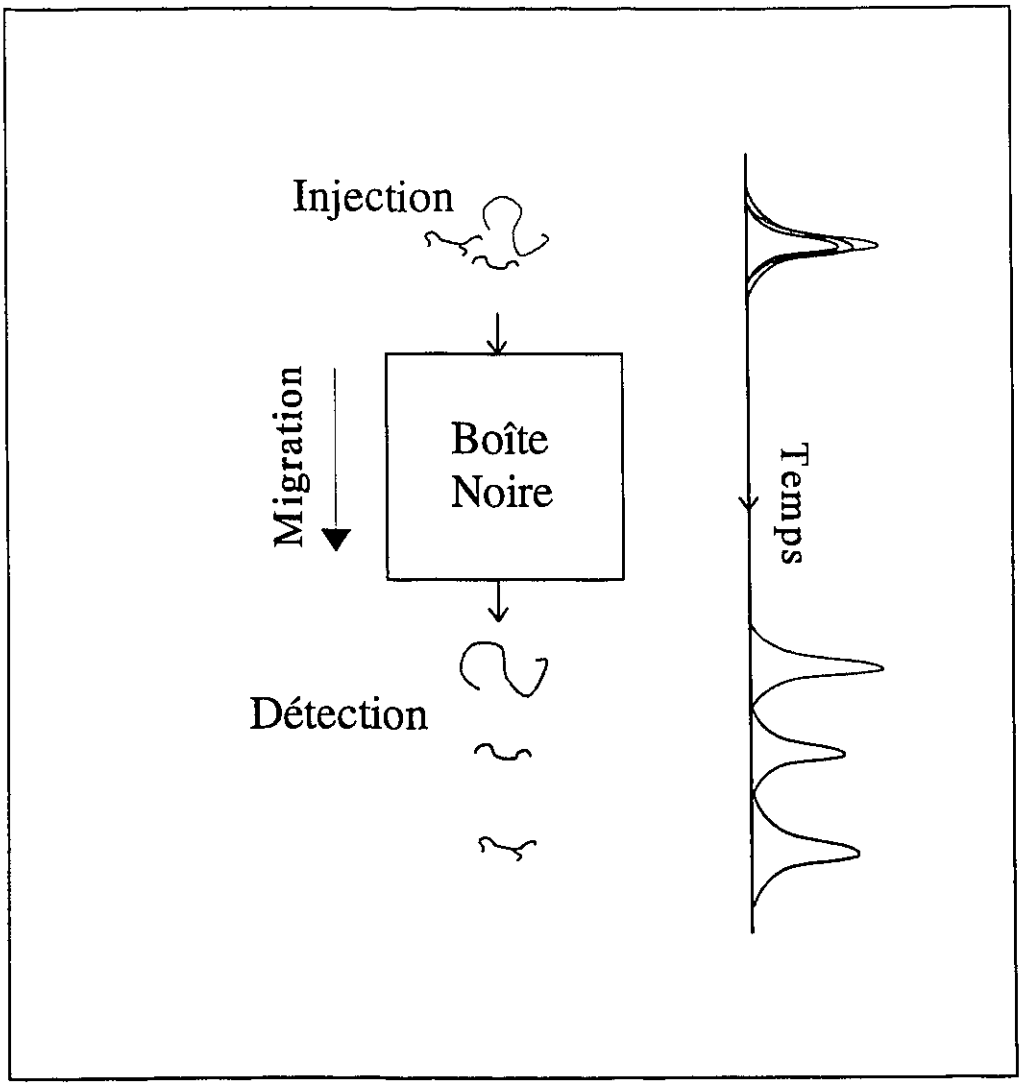

Figure 1.1 Représentation Schématique de l'Électrophorèse

molécule. Des publications récentes ont également démontré que l'ADN pouvait être séparé dans une solution de polymères ultra-diluée [8], ou encore en solution libre si on change son coefficient de friction en lui attachant un polymère neutre à un de ses bouts [9]. La troisième étape du processus de l'électrophorèse est la sortie des molécules. Lorsque ces molécules sont séparées, elles sont généralement détectées par un laser [8] ou par autoradiographie [15]. Le résultat final est une série de distributions (ou pics) que l'on doit interpréter. Une bonne séparation nous donne des distributions de masse éloignées les une des autres, et une bonne résolution nous donne des distributions de masse étroites par rapport aux écarts entre distributions.

1.2.2 Séparation dans un Gel

On emploie généralement un gel comme matrice de séparation pour l'électrophorèse de la molécule d'ADN. Un gel est une solution de polymères qui sont reliés entre eux par des liens fixes. La concentration de ces polymères est supérieure à la concentration d'enchevêtrement c* afin que ceux-ci puissent former une matrice. Nous pouvons également avoir une solution non-gélifiée où la concentration des polymères est supérieure à c*: dans ce cas, on parle plutôt de solution concentrée et non de gel, et les enchevêtrements entre les chaînes jouent le rôle des réticulations dans les gels.

On emploie un gel dans l'électrophorèse de l'ADN pour deux raisons importantes: (1) la rigidité et la haute densité du gel préviennent les effets de convection et de diffusion causés par le champ électrique, et (2) le gel introduit une séparation des micro-ions homologues tel que l'ADN qui ne peuvent être séparés en solution libre. Deux principaux gels sont utilisés comme milieu de séparation: le gel de polyacrylamide et le gel d'agarose. Même si le gel de polyacrylamide a démontré une excellente résolution (d'une paire de base) dans la séparation de l'ADN simple-brin jusqu'à une longueur de 450 bases, il peut seulement séparer des molécules d'ADN plus petites que ~2000 bases. Cette séparation s'effectue généralement en quelques heures (2-20) avec un champ électrique constant. Par ailleurs, le gel d'agarose est employé pour des masses moléculaires beaucoup plus grandes (ADN double-brin entre 2 kbp et 40 kbp) avec un champ électrique constant et de faible intensité. Le temps de séparation de ces grandes molécules peut atteindre plusieurs heures [16]. Présentement, la séparation de molécules plus grandes que 40 kbp est une des étapes les plus lentes dans le projet du génome humain. Ces séparations s'effectuent avec un champ électrique pulsé et emploient comme milieu de séparation le gel d'agarose; les temps de séparations atteignent facilement plus de 40 heures [7,17]. On peut conclure que le processus de l'électrophorèse dans un gel demande un travail acharné, beaucoup de temps, et qu'il implique plusieurs étapes de préparations afin d'obtenir une bonne séparation. Il reste également le problème de l'hétérogénéité du gel. Il est impossible de préparer un gel dont tous les pores sont énergétiquement équivalents [14,18]. Zimm et Lumpkin [19,20] furent les premiers à proposer une théorie sur l'électrophorèse de polyélectrolytes dans une matrice irrégulière suite aux résultats expérimentaux de Calladine, Collis, Drew and Mott [21]. Ces résultats sont incompatibles avec les théories présentement utilisées (modèle de la reptation biaisée [22] et modèle d'Ogston[23]). Le chapitre 4 nous donnera une brève description du modèle proposé par Zimm et Lumpkin [19] ainsi que la description d'une nouvelle approche que nous proposons. Il est donc nécessaire de trouver d'autres techniques de séparation de la molécule d'ADN ou d'améliorer grandement celles présentement utilisées.

Des techniques de séquençage plus rapides et plus simples seront aussi nécessaires pour que la génétique diagnostique devienne réalité.

1.2.3 Séparation dans une Solution Polymérique Concentrée, c>c*

En 1976, H.-J. Bode se servit d'une solution polymérique non gélifiée de cellulose d'acétate et de polyacrylamide comme matrice de séparation pour l'électrophorèse de macro-ions [24]. Un peu plus tard, Zhu et al. [25] et Chin et al. [26] ont reproduit l'expérience mais en effectuant l'électrophorèse dans un capillaire. Depuis, on a démontré l'utilité de plusieurs autres solutions polymériques dans la séparation de l'ADN (solution de glucomannane [27] , de polyéthylène glycol [28], de polyacrylamide linéaire [29,30], etc...). Par exemple, Strege et Lagu ont obtenu une excellente séparation pour des tailles moléculaires de 2 kbp - 23.1 kbp dans une solution visqueuse de 0.5% méthylcellulose [31]. Le mécanisme de séparation dans un tel système a été décrit par Grossman et Soane (1991) [32], ainsi que par Viovy et Duke (1993) [33]. La reptation reste le principal processus de déplacement des polyélectrolytes dans ces solutions [33]. Mais ce nouveau milieu de séparation ne nous permet pas de séparer d'énormes tailles moléculaires d'ADN. Sa performance équivaut alors à celle de l'électrophorèse en gel discutée auparavant.

1.2.4 Séparation dans un Capillaire

L'électrophorèse en capillaire est une technique de séparation qui a été introduite il y environ 10 ans (1983) [34]. Elle emploie un capillaire de verre dont le diamètre interne varie entre 25 et 100 μm et qui est rempli d'un gel (habituellement un gel de polyacrylamide). Cette méthode peut être jusqu'à 25 fois plus rapide que l'électrophorèse effectuée dans une plaque de gel pour la séparation d'ADN [35-40]. Sa reproductibilité et son efficacité à séparer les polyélectrolytes sont également supérieures. Mais malgré ces performances, cette technique récente n'est pas utilisée fréquemment par les biologistes moléculaires. La principale raison est l'aspect pratique de la plaque de gel. Par exemple, on peut faire la séparation de plusieurs colonnes de séquençage en parallèle dans une plaque de gel (jusqu'à 50), contre une seule dans un capillaire. Plusieurs groupes travaillent actuellement à développer un système de multiples capillaires en parallèle [41]; un fabricant vient d'ailleurs d'annoncer un modèle de 48 capillaires.

Un avantage majeur du capillaire est le ratio élevé de son aire de surface par rapport à son volume. Ceci permet de dissiper plus rapidement la chaleur produite par l'effet de Joule, ouvrant la voie

à l'utilisation de champs électriques beaucoup plus élevés [38] (400 V/cm pour le capillaire comparé à 100 V/cm pour la plaque de gel). Mais obtenir un gel uniforme dans un capillaire est très difficile. Même si un gel homogène est obtenu, des bulles peuvent facilement se former pendant l'électrophorèse. Mais puisque l'effet de convection est largement diminué, la structure rigide d'une matrice n'est plus nécessaire. On emploie donc souvent une solution polymérique concentrée (voir section précédente) ce qui est plus facile à préparer et à introduire dans le capillaire. Dans une publication récente, Barron et al. [8] ont démontré que des molécules d'ADN double brin pouvaient même être séparées dans une solution polymérique ultra-diluée dans un capillaire. En d'autre termes, la concentration c de polymères utilisée est largement inférieure à la concentration d'enchevêtrement c*. Le mécanisme de séparation dans un tel système semble être lié aux effets hydrodynamiques des polymères qui s'attachent temporairement à la molécule d'ADN durant sa migration dans la solution. Nous avons ont été les premiers à développer un modèle théorique pour expliquer les résultats de Barron et al. (ce sera le sujet du chapitre 3).

Récemment, nous avons aussi proposé de séparer la molécule d'ADN en solution libre en lui attachant un polymère neutre à un de ses bouts. Ce polymère se déformera dans le fluide changeant ainsi sa résistance, et modulant par le fait même la mobilité de la molécule d'ADN. Ce travail fera l'objet du chapitre 2.

1.3 Présentation de la Thèse

Tel que décrit précédemment, l'objet du chapitre 2 est d'étudier la dynamique d'un complexe ADN-polymère en solution libre. Le chapitre 3 introduit une nouvelle théorie sur la séparation de l'ADN en solution polymérique ultra-diluée et le chapitre 4 nous donne un aperçu de la dynamique de l'électrophorèse de l'ADN dans une matrice irrégulière. La conclusion de cette thèse se retrouve au chapitre 5.

Chapter 2

Theory of Capillary Electrophoretic Separation of DNA-Polymer Complexes*

2.1 Introduction

The rate at which DNA molecules can be sequenced using currently available technologies is the main obstacle of the human genome project. The separation techniques are based on gel electrophoresis which is a slow and time consuming process. The development of capillary electrophoresis (CE) has allowed the use of higher electric field intensities, leading to greatly reduced separation times; however, the process is still limited by the fact that separation of free-draining polyelectrolytes, such as DNA, requires the presence of a sieving matrix.

A radically new approach has been proposed over the last few years (see, e.g., [42] and [9]). In free-solution, the electric force acting on a DNA molecule is proportional to its size M_D (in bases) because each base carries the same electric charge. Its friction coefficient is also proportional to M_D because of its free-draining nature. Since the electrophoretic velocity is given by the ratio of the force to the friction coefficient (see Eq. (1.1)), it is molecular size-independent and no separation is possible under normal free-solution conditions. Instead of using a gel to introduce a size-dependence into the problem, one can change either the electric charge or the friction coefficient of the DNA. In principle, it is quite easy to change the total friction coefficient; for example, one needs only to attach an electrically neutral object to the DNA. This object will increase the friction and slow down the smaller DNA molecules more than the larger ones. Therefore, electrophoretic separation could be achieved without the use of a gel or any other polymer solution in a capillary. Moreover, very high field intensities could be used.

Mayer et al. [9] were the first to quantitatively study the physics of this idea, which they called ELFSE (End-Labeled Free Solution Electrophoresis). They concluded that if the object that is attached to the DNA molecule is a large globular molecule (such as a neutral protein) with a

---

* This work will be published in *Electrophoresis* in the fall of 1995.

well-defined friction coefficient, the electrophoretic separation of the hybrid molecules in a capillary and subject to high electric fields could increase the rate at which DNA can be sequenced by more than one order of magnitude. However, they did not study the case in which the friction-generating molecule to be attached to the DNA is a flexible neutral polymer. In this case, the polymer will deform in the flow and its hydrodynamic properties will change with the velocity of the DNA. Therefore, the analysis given in ref. [9] must be re-examined (for a flexible polymer). In this chapter, we present a detailed analysis of the hydrodynamic properties of such hybrid molecules in order to evaluate the feasibility of using polymeric friction-generating molecules for ELFSE of DNA.

This chapter is organized as follows. In Section 2.2 we present the main elements of our model; Section 2.3 describes our theoretical results for the hydrodynamics of the hybrid molecule. Our findings are then described in Section 2.4 in terms of velocity vs. molecular size diagrams. We conclude in Section 2.5 by examining some experimental strategies suggested by our analysis.

2.2 The Model

Figure 2.1 presents a schematic illustration of the problem: a DNA molecule and a neutral polymer chain are joined covalently to form a complex which drifts in the solvent under the influence of the electric field. Note that we do not explicitly consider the effect of the electro-osmotic flow here; in other words, the solvent is the frame of reference. The hydrodynamic resistance of the polymer to the drift will reduce the mean electrophoretic velocity of the DNA. This is a self-consistent problem since the deformation of the polymer under the flow will change its resistance to the drift. The net electrophoretic velocity of the complex and the hydrodynamic properties of the polymer molecule are thus intimately related.

The mean velocity V_{Dp} of a DNA-polymer complex can be written as:

$$V_{Dp}(M_D,\ M_p,\ E) = \frac{Q\,E - F_p(V_{Dp},\ M_p)}{M_D\ \xi_{D1}} \qquad (2.1)$$

Here, $Q \propto M_D$ is the effective charge of the DNA, E is the electric field intensity, F_p is the extra drag force acting on the DNA due to the polymer, M_D is the molecular size of the DNA (in

bases), ξ_{D1} is the DNA friction coefficient per base, and M_p is the size of the polymer (number of Kuhn lengths). Note that the denominator of Eq. (2.1) is not affected by the presence of the polymer since the effect of the polymer (extra-friction) is included in the term F_p. In order to calculate the mean electrophoretic velocity V_{Dp}, we must estimate the drag force F_p which is itself

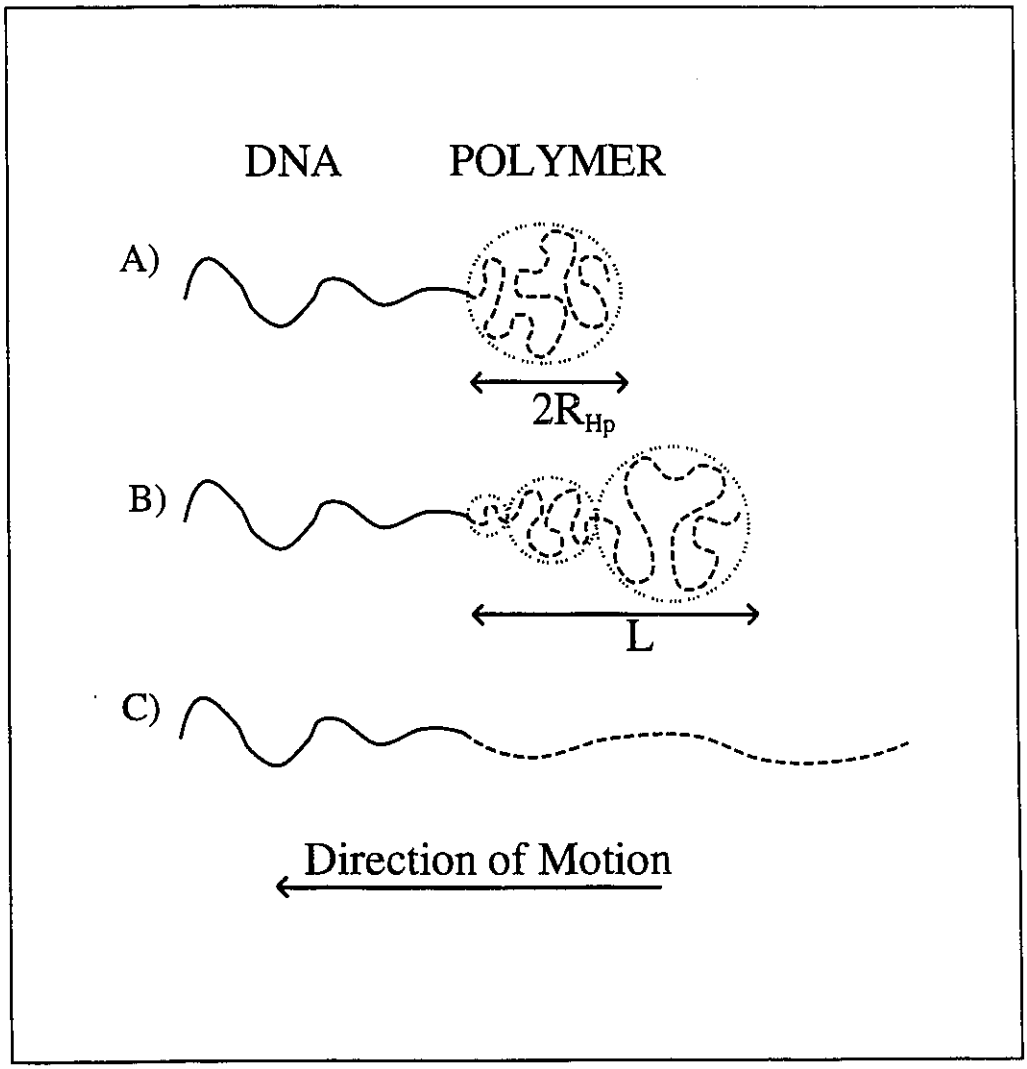

Figure 2.1 Conformations of the DNA-Polymer Complex
Schematic diagram showing the DNA-polymer complex in the three different regimes: (a) the polymer assumes a random coil conformation; (b) the polymer assumes a trumpet-like conformation; (c) the polymer is completely stretched. In each case, the DNA molecule is stretched because it must pull the large electrically neutral friction-generating polymer label.

a function of the velocity V_{Dp}. We thus have a self-consistent problem. It is also possible to write the problem in terms of the effective friction coefficient of the polymer molecule:

$$\xi_p = \frac{F_p}{V_{Dp}} \tag{2.2}$$

We then have the following expression

$$V_{Dp}(M_D, M_p, E) = \frac{Q\,E}{M_D\,\xi_{D1} + \xi_p} \tag{2.3}$$

It should be noted that Eqs. (2.1) and (2.3) are identical. If it is a rigid particle that is attached to the DNA, the extra friction coefficient ξ_p is an intrinsic property of the particle (it is independent of the velocity V_{Dp}); this is the basic idea presented in ref. [9] which showed that ELFSE was a workable alternative to standard gel electrophoresis. However, when we attach a deformable object (e.g. a polymer molecule) to the end of the DNA, this object can deform under the flow and its friction coefficient may become velocity dependent [i.e. $\xi_p=\xi_p(V_{Dp})$]. It is the goal of this chapter to examine this situation in detail.

The free-drift velocity V_0 of a bare DNA molecule is size-independent because DNA is a free-draining polymer. Following tradition, we will use the notation

$$V_0 \equiv \frac{Q\,E}{M_D\,\xi_{D1}} = \frac{q}{\xi_{D1}} \times E = \mu_0\,E \tag{2.4}$$

which defines $\mu_0=q/\xi_{D1}$ as the free-draining mobility of DNA, and $q=Q/M_D$ as the net charge per DNA base. Under typical experimental conditions, μ_0 is about 2.0 to 3.5 $\times$ 10^{-4} cm^2/Vs [43,44]. Experimental results are usually given as relative velocities (or mobilities) $V_{Dp0}\equiv V_{Dp}/V_0$.

2.3 Polymer Hydrodynamics

2.3.1 The Low-Velocity Regime

In this regime, the polymer is not deformed by the flow, that is, it remains in a coiled conformation (Fig. 2.1a). In this case, the polymer drag force F_p and friction coefficient $\xi_p=\xi^{coil}$ are given by [45]

$$\xi^{coil} = \frac{F_p}{V_{Dp}} = 6\ \pi\ \eta\ R_{Hp} \qquad (2.5)$$

where R_{Hp} is the hydrodynamic radius of the unperturbed polymer and η is the solvent (buffer) viscosity. The hydrodynamic radius of a polymer scales as follows [45]

$$R_{Hp} \cong M_p^{\nu}\ a_p \qquad (2.6)$$

where a_p is the Kuhn length of the polymer, and ν is the Flory exponent ($\nu=3/5$ for a polymer in a good solvent). The situation is quite simple because ξ^{coil} is not a function of the velocity; in other words, the polymer behaves much like a rigid object (a spherical coil which is impermeable to the solvent) in a weak flow. The results of ref. [9] are thus still valid. Using Eqs. (2.3), (2.4) and (2.5), we obtain the relative electrophoretic velocity

$$V_{Dp0} = \frac{V_{Dp}}{V_0} = \frac{1}{1 + \dfrac{\xi^{coil}}{M_D\ \xi_{D1}}} = \frac{1}{1 + \dfrac{M_\xi}{M_D}} \qquad (2.7)$$

where $M_\xi=\xi^{coil}/\xi_{D1}$ is the friction ratio. The relative electrophoretic velocity, V_{Dp0}, is a function of this ratio and the molecular weight of the DNA as obtained in ref. [9]. We also note that smaller DNA fragments are slower than longer ones.

The polymer coil starts to deform when the drag force F_p, as given by Eq. (2.5), exceeds the elastic force ($\approx k_BT/R_{Hp}$) that keeps the polymer in a coiled conformation [46-48]. Here, k_B is the Boltzmann constant, and T is the temperature. Therefore, Eq. (2.7) is valid only if

$$V_{Dp0} < \frac{V_{coil}}{V_0} \cong \frac{k_BT\ /\ \xi^{coil}\ R_{Hp}}{q\ E\ /\ \xi_{D1}} = \frac{1}{\epsilon_p} \qquad (2.8)$$

where V_{coil} is the critical velocity above which the polymer deforms. The scaled electric field intensity ϵ_p can also be written as

$$\epsilon_p \equiv \frac{M_\xi \, q \, E \, R_{Hp}}{k_B T} \tag{2.9}$$

We note that longer polymers deform more easily (i.e., at lower velocities) than shorter ones.

2.3.2 The High-Velocity Regime

In the opposite case, when the velocity is very large, the flow completely stretches the polymer (Fig. 2.1c). The friction coefficient is then given by [49]

$$\xi^{stretch} = \frac{F_p}{V_{Dp}} \approx 2 \, \pi \, \eta \, L_p \tag{2.10}$$

where $L_p = M_p a_p$ is the contour length of the polymer molecule (note that we have omitted a term of order $Log[L_p]$). Here, the situation is again quite simple since, as in the previous case, the friction coefficient of the polymer is velocity-independent. Equation (2.7) is thus replaced by

$$V_{Dp0} = \frac{1}{1 + \frac{\xi^{stretch}}{M_D \, \xi_{D1}}} \tag{2.11}$$

In a good solvent ($R_{Hp} \approx M_p^{3/5} a_p$), the relative electrophoretic velocity of the complex can than be expressed as

$$V_{Dp0} \approx \frac{1}{1 + M_p^{2/5} \times \frac{M_\xi}{M_D}} \tag{2.12}$$

However, since $L_p >> R_{Hp}$ (or, equivalently, $M_p >> 1$), we note that the resistance to the flow has increased substantially. Therefore, we are faced with a negative feedback situation in which a large velocity increases the friction coefficient of the polymer which, in turn, decreases the velocity. As we will see later, this has a profound impact on the velocity-molecular size relationship for particular situations.

2.3.3 The Intermediate Velocities

The deformation of the polymer chain depends on the external force acting on it. This force is proportional to the velocity of the flow of liquid around the polymer created by the motion of the DNA-polymer complex. In a weak flow (i.e., a low velocity as in Section 2.3.1), the polymer is an impermeable coil (Fig. 2.1a) and it adds a friction coefficient ξ^{coil} to the DNA; for very strong flows or very high velocities (as in Section 2.3.2), the polymer stretches completely (Fig. 2.1c) and adds a friction coefficient $\xi^{stretch}$ to the DNA. Between these two extremes, the polymer deforms in a succession of increasingly large impermeable blobs (Fig. 2.1b) whose individual friction coefficients one must add together [46-48]. This succession of "blobs" is called a trumpet conformation. We are following the ideas recently developed by Brochard-Wyart et al. [46-48] to describe the dynamics of a polymer chain in a strong flow; the polymer chain deforms from one blob to a series of blobs of increasing sizes (as shown schematically in Fig. 2.1b). In this case, the drag force acting on the polymer is given approximately by [46-48]

$$F_p \cong \eta\, L\, V_{Dp} \tag{2.13}$$

where L is the distance between the attached end and the free end of the polymer (see Fig. 2.1b), i.e. the length of the "trumpet-like" conformation. The elongation L of a polymer chain (or trumpet) in a good solvent is given by [46-48]

$$L(V_{Dp}, M_p) = M_p^3\, a_p^5 \left(\frac{\eta\, V_{Dp}}{k_B T} \right)^2 \tag{2.14}$$

which shows that the friction coefficient is now a function of the drift velocity V_{Dp}. From Eqs. (2.1), (2.13) and (2.14), we obtain

$$V_{Dp} \approx \frac{Q\,E - \eta\, V_{Dp}\, M_p^3\, a_p^5 \left(\eta\, V_{Dp} / k_B T \right)^2}{M_D\, \xi_{D1}} \tag{2.15}$$

The only real solution to this third order equation is

$$V_{Dp0} = \frac{V_{Dp}}{V_0} = \frac{\left(9\,x + \sqrt{12 + 81\,x^2} \right)^{2/3} - 12^{1/3}}{18^{1/3}\, x \left(9\,x + \sqrt{12 + 81\,x^2} \right)^{1/3}} \tag{2.16}$$

where

$$x \equiv \left(\frac{q\,E\,a_p}{k_B T}\right)\left(\frac{L_p\,\eta}{\xi_{D1}}\right)^{\frac{3}{2}}\frac{1}{\sqrt{M_D}} \qquad (2.17)$$

Interestingly enough, the solution of the problem is given in terms of a single dimensionless parameter which includes the field intensity E, the contour length of the polymer L_p, and the molecular size M_D of the DNA.

When $x \to 0$ and $x \to \infty$, Eq. (2.16) can be rewritten as:

$$\begin{aligned} V_{Dp0} &\approx 1 - x^2 + 3x^4 - O(x^6) && x < 1 \\ V_{Dp0} &\approx \frac{1}{x^{2/3}} - \frac{1}{3x^{4/3}} + \frac{1}{81x^{8/3}} + O(x^{-10/3}) && x >> 1 \end{aligned} \qquad (2.18)$$

Of course, these results are valid only if $V_{coil} < V_{Dp} < V_{stretch}$ (where $V_{stretch}$ is the velocity needed to completely stretch the polymer). If the velocity of the DNA-polymer complex is less than V_{coil}, the flow around the polymer is not strong enough to deform the polymer coil (see Section 2.3.1 and Fig.2.1a); for velocities above $V_{stretch}$, the flow is so strong that the polymer stretches completely (Section 2.3.2 and Fig. 2.1c). We can estimate the stretching velocity $V_{stretch}$ by solving Eq. (2.14) for $L(V_{Dp}, M_p) = L_p$, which gives

$$\frac{V_{stretch}}{V_0} \cong \frac{k_B T}{\eta\,L_p\,a_p} \times \frac{\xi_{D1}}{q\,E} \qquad (2.19)$$

In a good solvent, Eq. (2.19) can be rewritten using Eqs. (2.5), (2.6) and (2.9):

$$\frac{V_{stretch}}{V_0} \cong \frac{M_p^{1/5}}{\epsilon_p} \qquad (2.20)$$

It is interesting to note that $V_{stretch} \approx V_{coil} \times M_p^{1/5}$ for a polymer in a good solvent; therefore, the range of velocities in which the intermediate regime applies slowly increases with the size M_p of the polymer molecule.

2.4 Results

2.4.1 Low Field Intensities ($V_0 < V_{coil}$)

We saw that the electrophoretic velocity increases with DNA molecular size M_D for low field intensities (see Eq. (2.7)). If $V_0 < V_{coil}$, where V_{coil} is given by Eq. (2.8), not a single polymer is stretched by the flow (because V_0 is the maximum velocity a DNA molecule can reach) and Eq. (2.7) is valid for all DNA molecular sizes. Equation (2.8) indicates that this is the case for $\epsilon_p < 1$. Figure 2.2 shows how the relative velocity $V_{Dp0} = V_{Dp} / V_0$ then varies with the scaled molecular size m which is defined by

$$m \equiv \frac{M_D}{M_\xi} \tag{2.21}$$

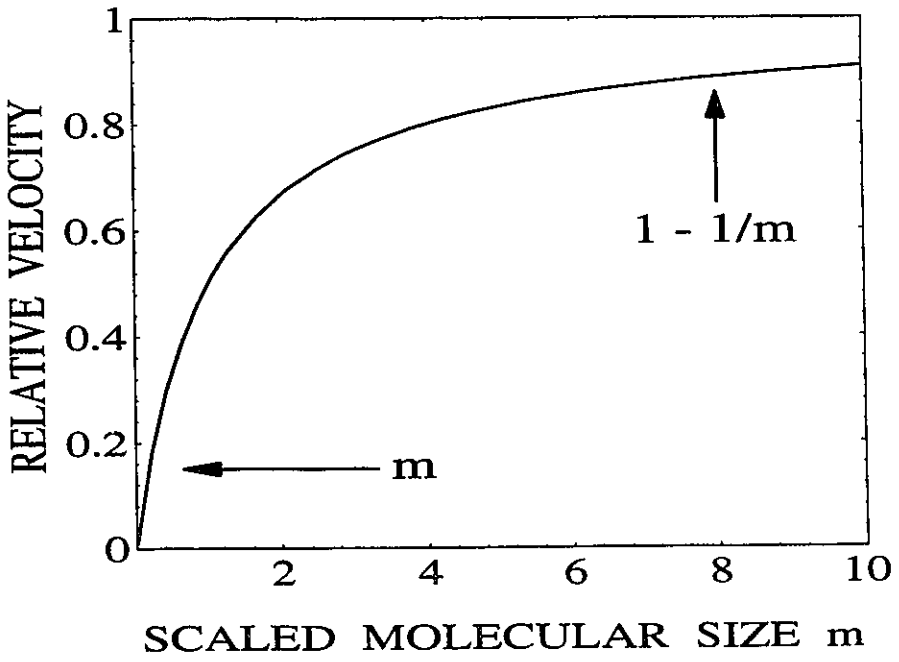

Figure 2.2 Relative Velocity vs. Molecular Size m for $V_0 < V_{coil}$
Relative electrophoretic velocity V_{Dp0} of the DNA-polymer hybrid molecule vs. the scaled DNA molecular size $m = M_D/M_\xi$ for a case where $V_0 < V_{coil}$. In this regime, the polymer retains its coiled conformation during the drift.

As shown in Fig. 2.2, we find the two simple limits

$$\begin{aligned} V_{Dp0} &\cong m && m << 1 \\ V_{Dp0} &\cong 1 - \frac{1}{m} && m >> 1 \end{aligned} \qquad (2.22)$$

Note that the exit time of the small molecules ($m << 1$) can be so large as to render ELFSE separations inefficient. There is a significant decrease in separation for large molecular sizes $m \gg 1$ (the curve is almost horizontal, indicating an essentially size-independent velocity). However, as we will see below, if the field is increased until the polymer starts to deform, one can increase the range of molecular sizes that can be separated since trumpets add more friction than coils. They do so using the negative feedback process that has been discussed previously.

2.4.2 Intermediate Field Intensities ($V_{coil} < V_0 < V_{stretch}$)

If the field intensity is large enough, the drift velocity of certain (large) molecules will exceed the critical velocity V_{coil} beyond which trumpets form. Using Eqs. (2.7) and (2.8), we find that the velocity V_{Dp} of an undeformed coil exceeds the critical velocity V_{coil} for DNA molecules larger than the critical (scaled) size

$$m_{coil} = \frac{1}{\epsilon_p - 1} \qquad (2.23)$$

We thus have two situations here: I) either $m_{coil} >> 1$, in which case the velocity required to form the trumpet is close to the maximum velocity V_0 (no appreciable gain is observed in the separation), or ii) $m_{coil} < 1$, and trumpet formation improves the separation. In the latter case, the velocity of the molecules with $m < m_{coil}$ still follows Eq. (2.7), while the dynamics of those with $m > m_{coil}$ is governed by Eq. (2.16).

In order to study these two cases, we note that Eq. (2.17) can be rewritten as

$$x \cong \frac{\epsilon_p}{\sqrt{m}} \qquad (2.24)$$

When the parameter $\epsilon_p < 1$, m_{coil} is negative (see Eq. (2.23)) and we simply recover the results of Section 2.4.1 (i.e., trumpets do not form). This is also predicted by Eq.(2.8). However, when $\epsilon_p \approx 1^+$, m_{coil} is very large and x is very small for all molecules with size $m > m_{coil}$. In this case, we can use the first expression of Eq. (2.18) together with Eq. (2.24) to obtain

$$V_{Dp0}(m) \cong 1 - \frac{1}{m} \tag{2.25}$$

which is identical to the second relation in Eq. (2.22). In other words, the polymer deforms only when they are attached to very large DNA molecules, but this deformation does not change the resolution. Thus, the separation process is not improved in this regime.

More interesting is the high field regime where $\epsilon_p >> 1$. In this case, m_{coil} is small and most molecules form trumpets. Using the second expression of Eq. (2.18) and Eq. (2.24), we obtain

$$V_{Dp0}(m) \approx \frac{1}{x^{2/3}} = \frac{m^{1/3}}{\epsilon_p^{2/3}} \tag{2.26}$$

This is a radical change from the first expression of Eq. (2.22); the relative velocity now increases only as the one third power of the molecular size of the DNA. Moreover, the velocity $V_{Dp} = V_{Dp0} \times V_0 \propto E^{1/3}$. The reason for these two results is simple: when the velocity increases (either because the DNA size increases or because the field intensity increases), the polymer trumpet extends and its friction coefficient increases; this slows down the DNA-polymer complex. This negative feedback loop makes the velocity increase only as the one third power of both M_D and E. This is a very important prediction of the model. Figure 2.3 shows that around $m = m_{coil}$, the velocity curve exhibits a dramatic shift in slope (this is a log-log plot). For very large sizes m, one reverts back to Eq. (2.24) since x then becomes smaller than unity. We also note in Fig. 2.3 that the trumpet regime actually increases the range of DNA molecular sizes m for which one can achieve good resolution (the velocity plateau is found for larger sizes m). One should therefore use high field intensities in order to deform the polymer.

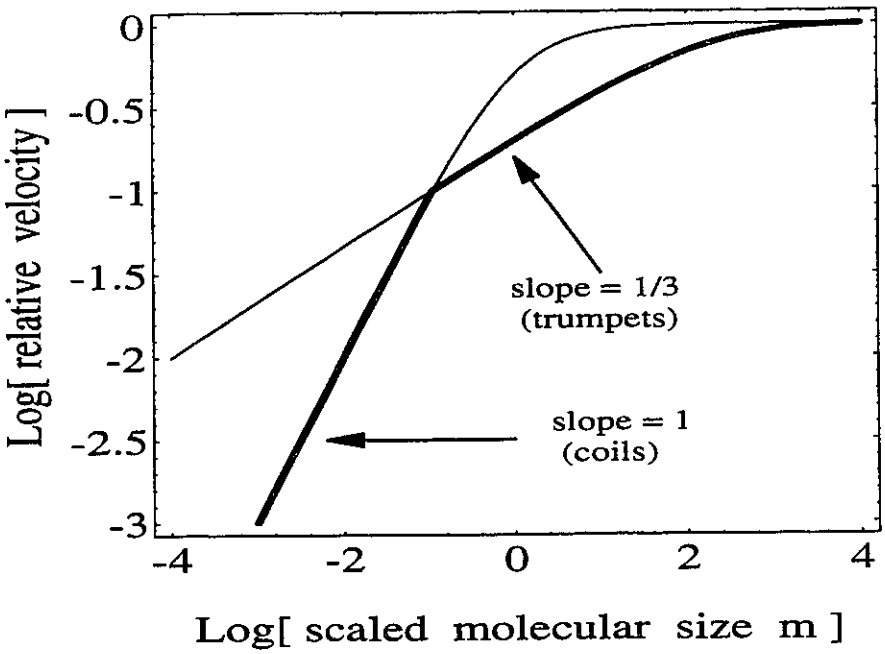

Figure 2.3 Relative Velocity vs. Molecular Size m for $V_0 < V_{stretch}$
Log-log plot of relative electrophoretic velocity V_{Dp0} of the DNA-polymer hybrid molecule (solid lines) vs. the scaled DNA molecular size $m = M_D/M_\xi$ for the case where the polymer undergoes a coil-to-trumpet transition at $m = m_{coil} = 1/9$. We chose $\epsilon_p = 10$ for this example. The slope is 1.0 for smaller molecules (Eq. (2.7) then applies), in agreement with Fig. 2.2; the slope is 1/3 for the DNA molecules that are large enough for the polymer to deform (Eq. (2.15) then applies). The change in slope at $m = m_{coil} = 1/9$ increases the range of molecular sizes that can be effectively separated. To facilitate comparison, the thin lines show Eqs. (2.7) and (2.15) for the range of sizes m where they do not apply anymore.

2.4.3 Strong Field Intensities ($V_0 > V_{stretch}$)

On the other hand, when the electrophoretic velocity of the DNA-polymer complex reaches the point where the polymer can stretch completely, one must use Eq. (2.11) to describe the system. We can calculate the critical (scaled) DNA molecular size (in a good solvent) where this transition takes place using Eqs. (2.12) and (2.20):

$$m_{stretch} \cong \frac{M_p^{3/5}}{\epsilon_p - M_p^{1/5}} \tag{2.27}$$

Therefore, if $\epsilon_p < M_p^{1/5}$, $m_{stretch}$ is negative and no DNA molecule is large enough to reach a velocity where its polymer section would completely stretch in the flow. However, if $\epsilon_p \approx M_p^{1/5} << M_p^{3/5}$, we find that $m_{stretch} \approx M_p^{2/5}$, which means that the polymer section will only stretch in the flow for extremely large DNA molecules; for $m > m_{stretch}$, Eq. (2.12) then becomes

$$V_{Dp0} \cong 1 - \frac{M_p^{2/5}}{m} \tag{2.28}$$

If we compare this relation with the second expression of Eq. (2.22) and Eq. (2.25), we see that the large molecular size ($m \gg 1$) behavior is essentially the same, except for the fact that the asymptotic velocity $V_{Dp0}=1$ is now approached more slowly (because $M_p >> 1$).

In the regime where $\epsilon_p > M_p^{3/5}$, the critical molecular size $m_{stretch}$ is small, which means that even small DNA molecules have their polymer section completely stretched; for $m > m_{stretch}$, Eq. (2.12) becomes

$$V_{Dp0} \cong \frac{m}{M_p^{2/5}} \tag{2.29}$$

Of course, this equation is similar to Eq. (2.22) for $m \ll 1$, except that the velocity increases more slowly with molecular size. This is due to the fact that stretched polymers have more resistance to the flow than coiled ones. Figure 2.4 illustrates a case in which the electric field intensity is such that we can observe all three regimes. For small (scaled) molecular size $m < m_{coil} = 1/3$, the polymer coil is not deformed and Eq. (2.7) is valid. For $m > 1/3$ and $m < m_{stretch} \approx 5/3$, the polymer molecule forms a trumpet and Eq. (2.16) applies. Finally, when $m > m_{stretch}$, the polymer is completely stretched and Eq. (2.12) applies. We can clearly see that the velocity increases more

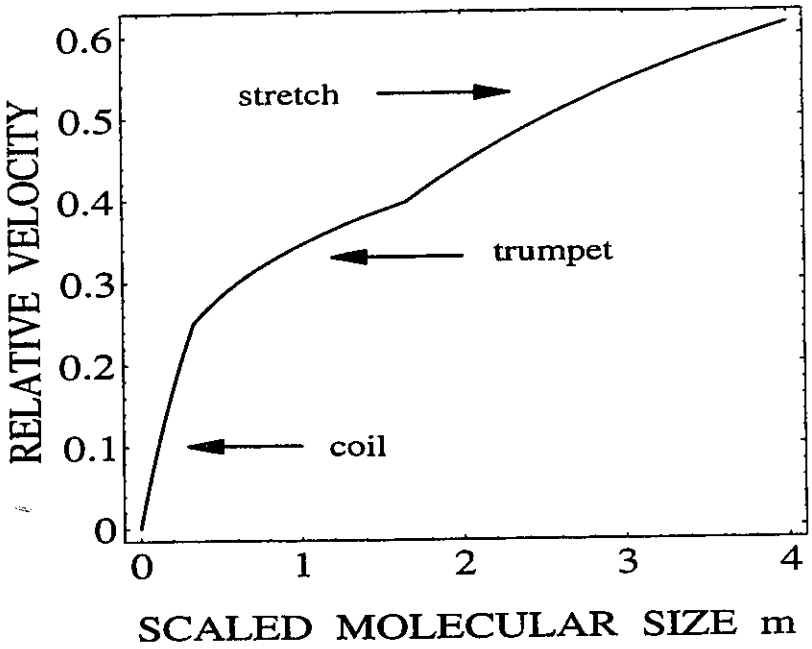

Figure 2.4 Relative Velocity vs. Molecular Size m
Relative electrophoretic velocity V_{Dp0} of the DNA-polymer hybrid molecule vs. the scaled DNA molecular size $m = M_D/M_\xi$. The parameters were $M_p = 10$ and $\epsilon_p = 4$. For small (scaled) molecular sizes $m < m_{coil} = 1/3$, the polymer is in a coil conformation and Eq. (2.7) applies. For $1/3 < m < m_{stretch} \approx 5/3$, the polymer begins to deform in a series of blobs (thus forming a trumpet-like conformation) and one must use Eq. (2.15). Finally, when $m > 5/3$, the polymer is completely stretched and Eq. (2.11) applies.

slowly in the intermediate regime; this is due to the negative feedback process we described earlier.

2.5 Discussion

We have presented a theoretical investigation of ELFSE for situations where the label is a flexible, neutral polymer. This study is based on the hydrodynamic theory of polymers in flows.

Let us briefly summarize our findings:

i) There are three main regimes (as depicted schematically on Fig. 2.1) characterized by the degree of polymer deformation induced by the flow.

ii) The properties of the dimensionless electrophoretic velocity V_{Dp0} can be understood in terms of a small subset of dimensionless parameters: the scaled DNA molecular size m, the scaled field strength parameter ϵ_p, and, finally, the polymer size parameter M_p.

iii) If $\epsilon_p < 1$, the polymer molecules are not deformed under the flow and we have a situation like the one shown in Fig. 2.1a, with the electrophoretic velocity given by Eq. (2.7). This is similar to the ELFSE case studied in ref. [9].

iv) If $1 < \epsilon_p < M_p^{1/5}$, the polymer molecules attached to the largest DNA fragments deform and assume a trumpet-like conformation as illustrated in Fig. 2.1b. The velocity is then given by Eq. (2.16). For smaller DNA fragments, case (iii) above still applies.

v) If $\epsilon_p > M_p^{1/5}$, the polymer molecules attached to the large DNA fragments stretch completely as shown schematically on Fig. 2.1c. The velocity is then given by Eq. (2.11). In this case, the previous two regimes are also observed for smaller DNA fragments.

Our theoretical analysis shows that a polymer molecule behaves very differently than a globular object when used as a friction-generating molecule for ELFSE. In fact, it allows one to obtain larger friction coefficients with smaller labels (because stretched polymers resist flow more so than do coiled ones). Moreover, the analysis provides us with an interesting trumpet-regime in which the velocity becomes less dependent upon both the electric field intensity and the DNA molecular size. Figures 2.3 and 2.4 clearly show that the range of DNA molecular sizes one can separate is larger in the intermediate (trumpet) regime than in the coil regime. Therefore, one of the main conclusions of our study is that the trumpet and the stretch regimes are of great interest for ELFSE.

Another remarkable finding is the behaviour of the hybrid molecule in the intermediate (trumpet) regime. We found that the free-flow velocity increases as $(QE)^{1/3}$. This is due to the fact that most of the extra electric force provided by larger DNA sizes and/or higher field intensities is used to deform the polymer and not to increase the net velocity. Since this power law ($E^{1/3}$) is predicted only for $m > m_{coil}$ (i.e., when $V_{Dp} > V_{coil}$), this offers a simple experimental method with

which to measure the coil deformation velocity V_{coil} of a polymer molecule. Similarly, we predict that the normal scaling law $V_{Dp} \propto QE$ is recovered if $m > m_{stretch}$ or $V_{Dp} > V_{stretch}$; this also provides a simple method for measuring the stretching flow velocity $V_{stretch}$ of a polymer molecule. We will approach a few experimental groups capable of doing these experiments in the near future.

Chapter 3

Theory of Capillary Electrophoretic Separation of DNA using Ultra-Dilute Polymer Solutions*

3.1 Introduction

Modern genetics relies heavily on electrophoresis to separate DNA molecules of different molecular sizes. In free liquid, DNA migrates at a velocity which is independent of its molecular weight. It is for this reason that size separations are generally performed in gels [6]. The separation process is usually described (at least qualitatively) by either the so-called Ogston sieving model [50] (when the DNA molecules are small compared to the typical pore size of the gel) or the reptation model [51-53] (which applies to larger molecules which must migrate end first through the gel structure). Gel electrophoresis is labor-intensive and poorly reproducible, so considerable efforts are currently focussed on using capillary electrophoresis (CE) in which DNA separation can be achieved in uncrosslinked, entangled polymer solutions ($c > c^*$) [10]. The mechanism of this process was shown to be related to reptation (see ref. [33]). Recently, the experimental results of Barron et al. [8] have demonstrated that separation can also be achieved in unentangled, ultra-dilute polymer solutions ($c << c^*$) of hydroxyethyl cellulose (HEC). For example, large DNAs (2-23 kbp) were separated by CE using a high electric field (270 V/cm) and HEC polymer mass concentrations as low as 0.0006%, although c^* was estimated to be near 0.40% for this sample (90000-105000 average molecular weight (MW) HEC). Since a network of entanglements cannot exist for $c << c^*$, standard models cannot explain these surprising results. We were the first to suggest a quantitative theory to explain these revolutionary results.

This chapter is organized as follows; in Section 3.2 we present the main elements of the model; Section 3.3 describes the polymer relaxation and collision processes; the ultra-dilute regime is described in Section 3.4 in terms of velocity vs. molecular size relationships; solutions of longer polymers are discussed in Section 3.5; we then conclude in Section 3.6 by examining

---

*This work has been accepted for publication by *Macromolecules* (Oct 1995).

some experimental strategies suggested by the analysis.

3.2 The Model

Figure 3.1 presents a schematic illustration of the separation process as suggested by Fig. 7 of ref. [8]. In this model, we assume that a DNA molecule temporarily "captures" the polymers with which it collides during its electrophoretic drift. Clearly, these polymers resist the flow and slow down the migration of the DNA. However, the captured polymers also deform under the flow. This, in turn, affects their resistance to the flow. The net electrophoretic velocity of the DNA molecule and the hydrodynamic properties of the polymers are thus intimately related. In

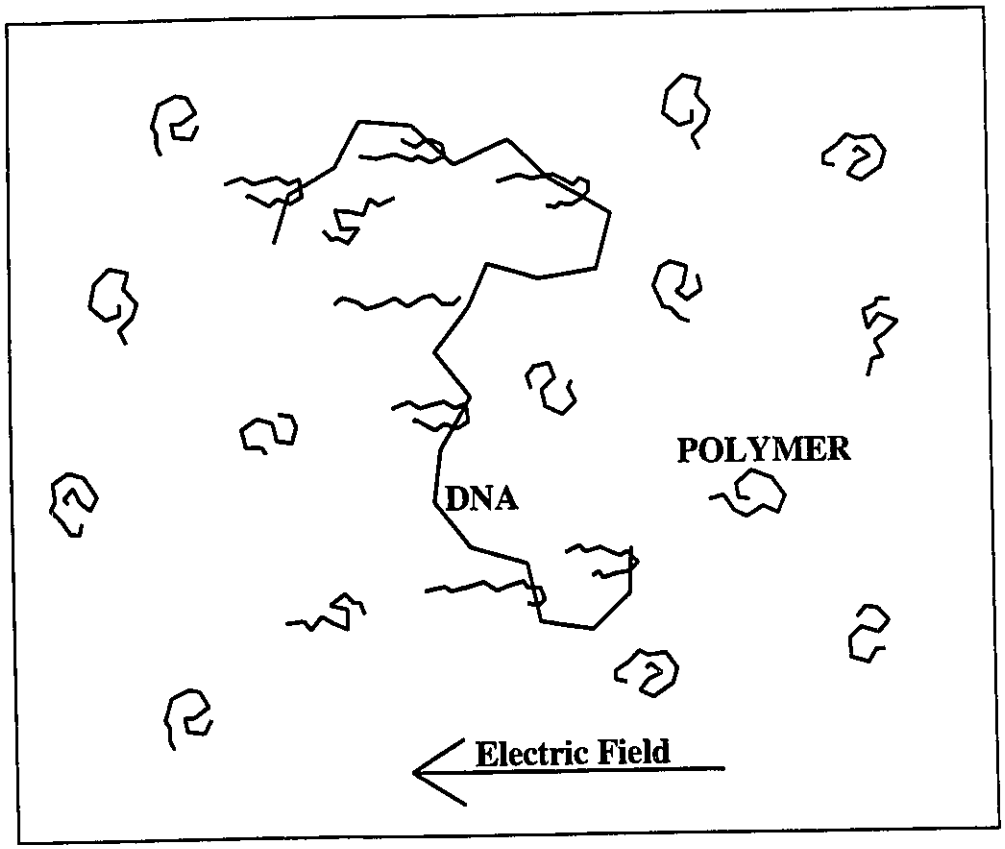

Figure 3.1 Representation of the DNA Molecule during Electrophoresis
Schematic illustration of the DNA molecule during electrophoresis in a dilute solution of polymers (e.g. 24000-27000 average MW HEC) as suggested by Fig. 7 of ref. [8]. We note that the radius of gyration of the polymer is smaller than the persistence length of the DNA. The electro-osmotic flow is not taken into account.

this chapter, we describe the main features of the process described earlier (see Fig. 3.1), and we focus our attention on the 24000-27000 average MW HEC case studied in [8]. For simplicity, we work in the frame of reference in which the free HEC molecules are at rest, which means that the contribution of the electro-osmotic flow does not appear explicitly; our results can therefore be compared directly with those of ref. [8].

The capture and release of polymers (e.g., HEC) is at the heart of the separation phenomenon. We denote the mean number of polymers in contact with a DNA molecule by n. Two distinct regimes can be identified in this problem; either there is, on average, less than one polymer molecule ($n < 1$) in contact with the DNA, or we have $n >> 1$ (the most significant regime). In the latter case, we can assume a steady-state situation, meaning that the number of polymers entangled around a DNA molecule is constant.It is clear that the $n < 1$ regime will be less efficient than the $n >> 1$ regime wherein each DNA fragment drags along many polymer molecules. In the former case ($n < 1$), the effect of the polymer molecules is much smaller (possibly negligible), and the large fluctuations of the DNA velocity (the DNA is free-drifting part of the time, but also drags a polymer molecule some of the time) are expected to lead to broad electrophoretic bands or peaks. In the other case ($n >> 1$), one can define a steady-state value of n, and the large number of polymers per DNA insures a large effect and smaller fluctuations (narrower electrophoretic peaks). We can write the mean electrophoretic velocity V_D of a DNA molecule for $n \geq 1$ as:

$$V_D = V_n = \frac{Q\,E - n\,F_{drag}}{M_D\,\xi_{D1}} \qquad (3.1)$$

where Q is the effective charge of the DNA, E is the electric field intensity, F_{drag} is the average drag force acting on the DNA due to one polymer, M_D is the molecular size of the DNA (in base pairs, or bp), and ξ_{D1} is the DNA friction coefficient per bp. The denominator of Eq. (3.1) is not affected by the presence of the polymer since the effect of the polymer (extra-friction) is included in the term F_{drag}. Note that Eq. (3.1) is identical to Eq. (2.1) for n equal to 1. However, the two situations are quite different; in the previous case, the DNA molecule dragged a neutral polymer that was covalently attached to it whereas here, the DNA molecule drags n polymers that are temporarily entangled around it. Also note that for $n=0$, we recover Eq. (2.4), which defines the

free-drift velocity of the DNA.

When $0<n<1$, the polymer/DNA collisions are separated by periods during which the DNA drifts freely, and we have, instead,

$$V_D = \frac{V_{n=1}\,\tau + (\tau_{coll} - \tau)\,V_{n=0}}{\tau_{coll}} \qquad (3.2)$$

where $V_{n=1}$ and $V_{n=0}$ are given by the right-hand side of Eq. (3.1), τ is the mean lifetime of one polymer-DNA contact, and τ_{coll} (with $\tau_{coll} \geq \tau$) is the mean time between collisions. Therefore, in order to calculate V_D, we must estimate the collision time τ_{coll}, the escape time τ, the mean drag force F_{drag}, and, finally, the mean aggregation number n.

Since the experimental results are usually given as relative velocities (or mobilities), $v=V_D/V_0$, we will rewrite Eqs. (3.1) and (3.2) as:

$$\begin{aligned} n>1; \quad & v = 1 - n \times \frac{F_{drag}}{Q\,E} \\ n<1; \quad & v = 1 - \frac{\tau}{\tau_{coll}} \times \frac{F_{drag}}{Q\,E} \end{aligned} \qquad (3.3)$$

These equations represent the starting point of our calculations. The effect of the polymer solution are contained in the last term.

3.3 Polymer Relaxation and Collision Processes

3.3.1 Polymer Collisions

The mean aggregation number n can be estimated using a simple rate equation that takes into account both the DNA-polymer collision rate and the mean escape rate of captured polymer molecules. This equation reads:

$$\frac{dn}{dt} = \frac{1}{\tau_{coll}} - \frac{n}{\tau} \qquad (3.4)$$

where $1/\tau_{coll}$ is the mean number of collisions between a migrating DNA molecule and the free polymer molecules per unit time. In the steady-state (which is the case when $n>>1$), one has

$dn/dt = 0$ and the solution of this rate equation gives:

$$n = \frac{\tau}{\tau_{coll}} \tag{3.5}$$

This results indicates that the aggregation number n is larger when the captured polymer molecules disengage very slowly and/or the collision rate is large. It also indicates that the two expressions in Eq. (3.3) are actually identical. The escape time τ is discussed in the next section. The collision rate $1/\tau_{coll}$ is simply given by:

$$\frac{1}{\tau_{coll}} = V_{bc}\ c\ S \tag{3.6}$$

where S is the collision cross-section between the DNA molecule and the free polymer molecule, c is the polymer number concentration, and V_{bc} is the drift velocity of the DNA molecule between collisions. One can also note that the product of the velocity and the collision cross-section S is simply the volume scanned by the DNA molecule per unit of time. Clearly, $V_{bc} = V_0$ if $n << 1$ while $V_{bc} = V_D$ (the steady-state situation) if $n >> 1$.

The collision cross-section S depends on the molecular size and flexibility of both macromolecules. We have two different cases (the contour lengths of both macromolecules are considered much longer than their own persistence length such that both polymers are flexible). Of foremost importance is p, the persistence length of the DNA ($p \approx 60$ nm, corresponding to about 200 bp), and, R_p, the radius of gyration of the polymer in solution (for the 24000-27000 MW HEC, $R_p \approx 27$ nm). When $R_p < p$, the polymer collides with only one DNA segment at a time and the collision cross-section S is given by

$$S \cong R_p \times L_D \tag{3.7}$$

where L_D, the contour length of the DNA molecule, is given as

$$L_D = M_D\ a_D \tag{3.8}$$

with M_D the number of base pairs (bp) of the DNA molecule and a_D the length of one base pair ($a_D \approx 0.34$ nm).This will be the case of interest here. In the other case, where $R_p > p$, the collision process can involve many DNA segments simultaneously, and the collision can be seen as involving two rigid objects (spheres), with

$$S \cong \text{Max}\left[R_p^2, R_D^2 \right] \tag{3.9}$$

where R_D is the radius of gyration of the DNA molecule. This expression indicates that we can expect a change of behavior when the radius of gyration of the DNA is close the size of the radius of gyration of the polymer.

3.3.2 Polymer Relaxation

Assuming that both the DNA and the polymer slide around their point of contact (see Fig. 3.2), the mean lifetime (or escape time) τ is given by

$$\frac{1}{\tau} = \frac{1}{\tau_p} + \frac{1}{\tau_D} \tag{3.10}$$

where τ_D is the time required for the DNA molecule to disengage from the polymer, and τ_p is the time required for the polymer to disengage from the DNA. It is important to realize that both disengagement processes are active at the same time.

The escape time of a (pulley-like) DNA molecule around an obstacle has been studied by many authors [54-56]; simple arguments indicate that it simply scales as follows:

$$\tau_D \approx \frac{L_D}{2\, V_n} \tag{3.11}$$

The polymer also slides around the DNA molecule because of the unequal drag forces acting on the two legs of the U-shaped conformation. These forces critically depend on the contour length L_p of the polymer and the intensity of the electric field E. The work of Brochard-Wyart et al. [47-48,57] suggests that for low field intensity/low velocity, one should expect the polymer to assume a "trumpet-like" conformation (Fig. 3.2) because the drag forces are not

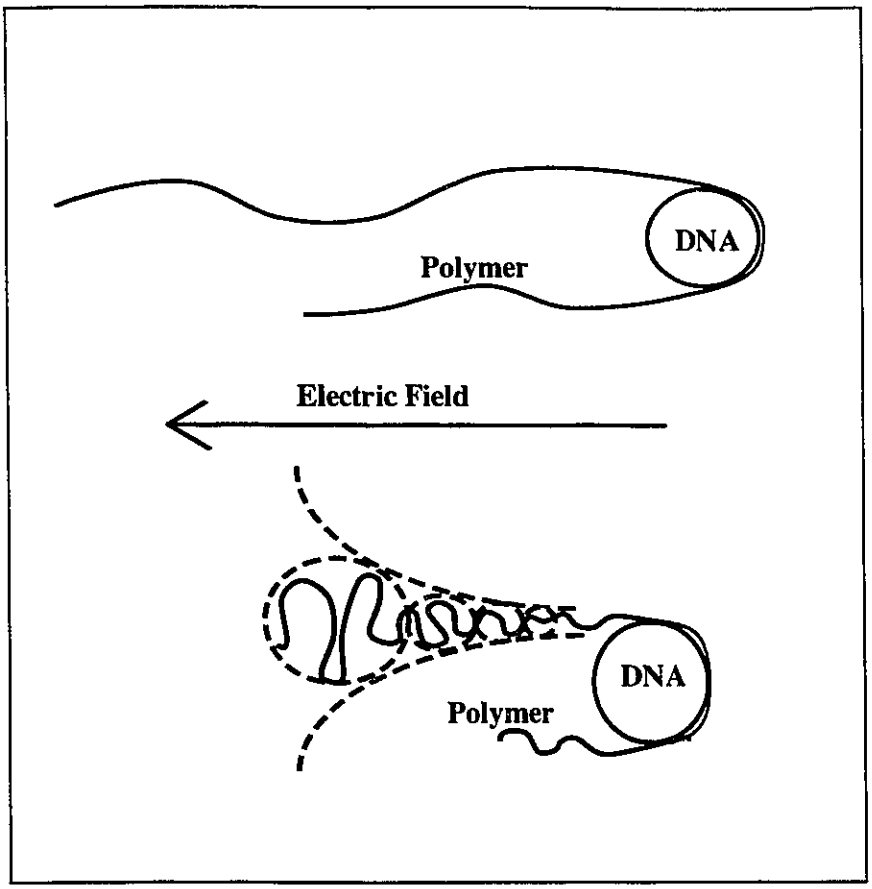

Figure 3.2 Polymer Dragged by a DNA Molecule
Schematic illustrations of the conformations of a polymer which has been captured by a DNA molecule. The upper figure represents the high field intensity/large velocity case where the polymer is almost completely stretched. The bottom part represents the low field intensity/low velocity case where the polymer is in a "trumpet-like" conformation. In both cases, the longest arm of the polymer "pulley" grows at the expense of the small one until the polymer disengages from the DNA molecule. At the same time, the DNA also forms a pulley and slides around the polymer.

sufficient to fully stretch the polymer. This case will not be treated here. For high field intensities, the polymer stretches almost completely (see Fig. 3.2). This is also a pulley-like problem where the difference in the frictional forces on the two arms of the captured polymer causes the longest arm to grow at the expense of the short one until the polymer escapes. The differential equation related to this problem is given by

$$L_1 \left(V_n - \frac{dL_1}{dt} \right) - (L_p - L_1) \left(V_n + \frac{dL_1}{dt} \right) = 0 \qquad (3.12)$$

where L_1 is the contour length of the longest arm of the U-shaped conformation, and V_n is the velocity of the polymer(s)-DNA aggregate during the disengagement process. Note that we have canceled a factor $2\pi\eta$ from each of the three terms, where η is the viscosity of the buffer solution. The first term of this equation measures the drag force applied by the longest arm, while the second term refers to the shortest arm. The solution to the equation is:

$$L_1(t) = \left(L_1(0) - \frac{L_p}{2} \right) e^{2 V_n t / L_p} + \frac{L_p}{2} \qquad (3.13)$$

where we assumed that the velocity of the aggregate (V_n) is constant during the escape process (this is a good approximation when $n >> 1$). The average escape time τ_p is defined by the condition that $L_1(\tau_p) = L_p$. We then average this result over a uniform distribution for $L_1(0)$, with $L_p/2 < L_1(0) < L_p$, to obtain the mean polymer escape time,

$$\tau_p \cong \frac{L_p}{2 V_n} \qquad (3.14)$$

We note that the relaxation time for the polymer molecules is similar to that given in Eq. (3.11) for the DNA molecule.

3.3.3 Polymer Drag Forces (for stretched polymers)

The instantaneous drag force on the DNA molecule due to one polymer can be expressed as the sum of the two terms in the l.h.s. of Eq. (3.12):

$$F_{drag}(t) = 2 \pi \eta L_1 \left(V_n - \frac{dL_1}{dt} \right) + 2 \pi \eta (L_p - L_1) \left(V_n + \frac{dL_1}{dt} \right) \qquad (3.15)$$

The mean drag force for a given initial condition $L_1(0)$ is the average of $F_{drag}(t)$ over the period

of time t=0 to τ_p (i.e. over the whole escape process), with $L_1=L_1(t)$ being given by Eq. (3.13). We then average the result over a uniform distribution of initial lengths $L_1(0)$, with $L_p/2 < L_1(0) < L_p$, to obtain the mean drag force applied by a polymer to the DNA molecule:

$$F_{drag} \cong \eta\, L_p\, V_n \tag{3.16}$$

If the velocity V_n cannot be assumed to remain approximately constant during the escape process, one has to solve for F_{drag}, τ_p and V_n simultaneously. This will not be discussed since only the $n>>1$ case is relevant to explain the results of ref. [8].

3.4 The Ultra-Dilute Regime ($n>>1$)

This is the regime in which the average number of polymers dragged by a DNA molecule can be considered constant. In this regime, it is assumed that we have a steady-state velocity and that the collision cross-section is constant. The mean electrophoretic velocity can be derived using Eqs. (3.1), (3.5), (3.6), (3.10), (3.11), (3.14) and (3.16):

$$v = \frac{V_D}{V_{n=0}} \approx \frac{1}{1 + \dfrac{\gamma' C S}{M_D} \times \left(1 + \beta \dfrac{L_p}{L_D} \right)^{-1}} \tag{3.17}$$

where $C \propto L_p c$ is the HEC concentration in the units of ref.[8], and $\gamma' \propto L_p$ and β are parameters which depend on the characteristics of both polymers (HEC, DNA), but do not depend on DNA size. We will now compare our results to those of Barron et al. [8] for the 24000-27000 MW HEC polymer solutions to which Eq. (3.7) applies. For this case, we can rewrite Eq. (3.17) as

$$v \approx \frac{1}{1 + \gamma C \left(1 + \beta \dfrac{L_p}{L_D} \right)^{-1}} \tag{3.18}$$

The parameter γ, which is proportional to $\gamma' R_p$ ($\propto L_p R_p$), can be estimated as follows. Figure 3.3 shows $[1/v]-1$ vs C for $M_D \to \infty$ as obtained from ref. [8]. According to Eq. (3.18), this plot should yield a straight line of slope γ. The figure is in good agreement with this prediction (where we obtain $\gamma \approx 0.95$). In order to obtain β, we use Eq. (3.18) to fit ref. [8]'s velocity vs. concentration data for various DNA molecular sizes with $\gamma \approx 0.95$ and $L_{HEC=24000} \approx 51.5$ nm. As can be seen in the insert of Fig. 3.3, β is essentially constant for DNA molecules larger than one persistence length ($M > 200$ bp). The figure clearly indicates the existence of a different regime for smaller DNA molecules although this will not be studied here. Using the mean value $\beta = 1.76$, Eq. (3.18) yields the solid lines found in Figs. 3.4 and 3.5. We can see that our expression is in good

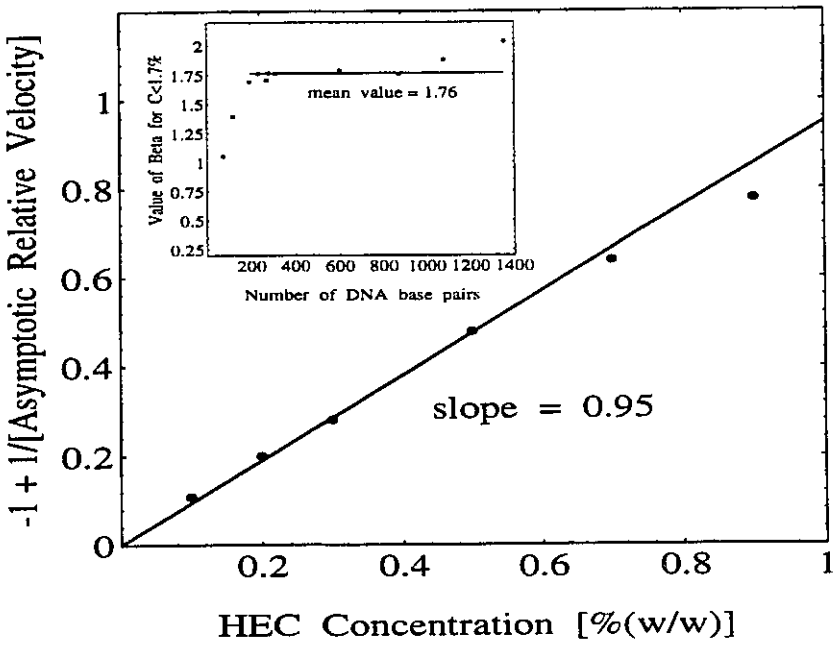

Figure 3.3 Values of γ and β
Plot of $[-1+V_{n=0}/V_D(M_D \to \infty)]$ vs. the HEC concentration C; the slope gives the parameter γ. The asymptotic velocities $V_D(M_D \to \infty)$ were estimated from the raw data of ref. [8]. The insert shows the value of the parameter β vs. DNA molecular size. The mean value for $M_D \geq 200$bp is about 1.76.

agreement with the experimental results when $C < C^*$ ($\approx 1.8\%$ for this case) and $M_D > 200$ bp. Deviations are found for very low concentrations C. This is possibly due to the fact that Eq.(3.1) is no longer valid in this case and should be replaced by Eq. (3.2).

From Eq. (3.18), we can compute the optimum HEC polymer concentration for separating DNA molecules of size M_D by solving the equation $\partial^2[v] / \partial C \partial M_D = 0$. The derivative vs. the mass simply gives the difference in electrophoretic velocity between two sizes. The second derivative over the concentration gives us the optimum concentration needed to maximize that difference. We thus obtain:

$$C_{optimum} = \frac{1}{\gamma} + \frac{\beta L_p}{\gamma L_D} \qquad (3.19)$$

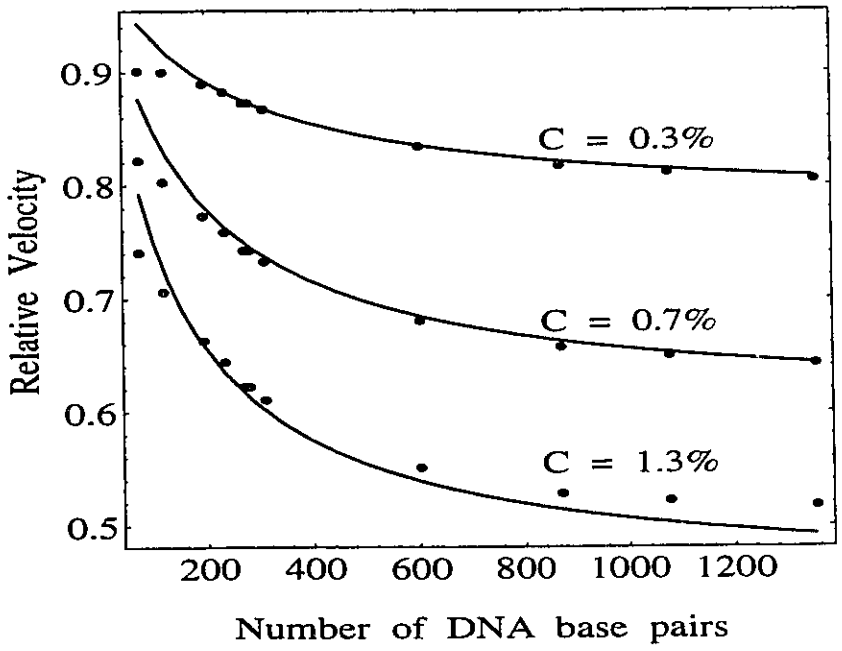

Figure 3.4 Relative Velocity vs. Number of DNA Base Pairs
Plot of the relative velocity $V_D(M_D)/V_{n=0}$ vs. molecular size M_D of the DNA (in bp). The experimental points come from ref. [8]. The solid lines are obtained from Eq. (3.18).

The insert of Fig. 3.5 shows that Eq.(3.19) is in fair agreement with experimental results considering the number of approximations made, the uncertainty of the data points, and the fact that this comparison between the second derivatives involves no curve-fitting. Note in particular that our results agree with the fact that the optimal concentration plateaus for very large DNA sizes (one of the most important qualitative results in [8]). Since $\gamma \propto R_p L_p \propto L_p^{8/5}$, we also predict that the optimal concentration for the separation of large DNA molecules $C_{optimum}(M_D \to \infty)$ will decrease as the 8/5-th power of the molecular size of the HEC molecules. For the 95000-105000

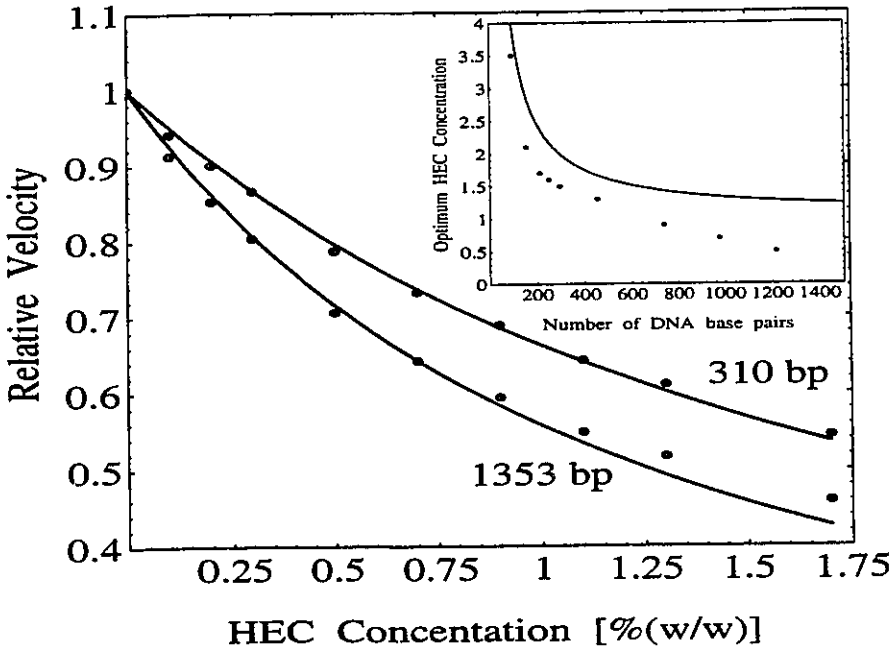

Figure 3.5 Relative Velocity vs. HEC Concentration
Plot of the relative electrophoretic velocity of the DNA molecule $V_D/V_{n=0}$ vs. the HEC concentration C. The experimental points come from ref. [8] (upper points for M_D=310 bp, and lower points for M_D=1353 bp). The solid lines are obtained from Eq. (3.18). The insert shows a plot of the optimum HEC concentration vs. the size of the DNA molecule to be separated (in bp). The experimental points come from ref. [8]; the solid line comes from Eq. (3.19).

average MW HEC used in [8], we thus predict that the plateau value $C_{optimum}(M_D \to \infty)$ should be a factor of about $4^{8/5} \approx 9$ smaller than for the 24000-27000 MW HEC polymer solutions. Barron et al. [8] found roughly $C_{optimum} \approx 0.5\%$ in the later case, and 0.05% in the former case, giving a ratio of about 10 which compares well with our predictions.

3.5 Using Longer Polymers

The mean electrophoretic velocity of the aggregate given by Eq. (3.18) plateaus for very large DNA molecular weights. This was observed by Barron et al. for small polymers, namely the 24000-27000 MW HEC solutions. On the other hand, if the polymers are much longer, for instance the 95000-105000 average MW HEC used in [8] ($R_p \geq p$), we can use Eqs. (3.17) and (3.9) to obtained a relationship for the electrophoretic velocity. For large DNAs (where $R_D >> R_p$), we find the following asymptotic behaviour:

$$\frac{V_D}{V_{n=0}} \propto \frac{1}{C\, M_D^{1/5}} \tag{3.20}$$

Since $V_D \propto M_D^{-1/5}$, it suggests that we can separate very long DNA (Mbp) molecules without the complex pulsed field gel electrophoresis techniques now used. This is qualitatively consistent with the results of Barron et al. [8] who did not observe a plateau for the large DNA molecules. The $M_D^{-1/5}$ power-law indicates a weak dependence upon molecular size, but this could be enough to separate a few Mbp-sized molecules (e.g., yeast chromosomes) with low resolution.

3.6 Discussion

Our model can be generalized to treat numerous other cases: (i) large polymers have different collision cross-sections than smaller ones with DNA; (ii) small DNAs are too rigid to form pulley conformations and "slide" around the point of contact with the polymer; (iii) lower field intensities and/or smaller DNA velocities may lead to cases where a polymer assumes a trumpet-like conformation which will greatly modify the escape time τ_p and the mean drag force F_{drag}; (iv) if the polymer concentration C is very low, one has, on average, less than one polymer attached per DNA molecule and Eq. (3.2) must be used instead of Eq. (3.1). In the latter case,

the velocity of the DNA changes during the escape process which means that the escape times, the mean drag force, and the mean DNA velocity must be calculated self-consistently. In this case, one must also take into account the finite relaxation time of the DNA between two collisions since it may lead to a collision cross-section S that changes with time. Finally, the polymer-polymer and DNA-DNA hydrodynamic interactions have been neglected.

The simple model presented here with the scaling relations for the escape times, mean aggregation number, and mean drag force per polymer, explains the surprising results reported by Barron et al. [8] for 24000-27000 average MW HEC polymer solutions. These results cannot be expected to follow a simple extension of either the Ogston or the reptation model. Therefore, we have mathematically described a yet unknown separation mechanism (consistent with the qualitative picture proposed by Barron et al. [8]) which is based on hydrodynamics, molecular collisions and drag forces. At the present time, the limits of this new separation mechanism are unknown. We are exploring the various scenarios one might use to increase the correlation between the total drag force and the molecular size of the DNA molecules. However, it is already clear that the net velocities permitted by this mechanism are much larger than when performing standard gel-based separations. If a similar resolution could be achieved in dilute solutions, this would represent a major advance in DNA separation techniques. Because of the type of molecular conformations the DNA and the polymers assumed during their association (Fig. 3.2), it is possible that pulsed fields may reduce the mean lifetime of the polymer-DNA contacts, thus offering an alternative method to modulate the effect of the drag forces on selected DNA molecules.

Chapter 4

A Reptation Model with Random Local Interactions

4.1 Introduction

DNA gel electrophoresis is usually described by either the Ogston [23] or the reptation model [51-53]. For small DNA fragments whose radius of gyration R_G is smaller than the average gel pore size a, the Ogston model is normally used. In this regime, the polymeric macro-ion is assumed to migrate through the gel as an unperturbed spherical coil. For DNA coils much larger than the typical pore size, the model predicts that the polymer will not enter the gel at all; however this is contrary to experimental observations. Thus the geometrical assumptions of the original Ogston model are not valid for large DNA molecules ($R_G > a$). It is clear that these molecules must stretch and change shape to move through the gel. The biased reptation model was developed to explain the behavior of such DNA coils which are too large to fit into a single gel pore during gel electrophoresis. The original reptation model was in fact developed to explain the thermal diffusion of linear polymers (such as polystyrene) in a concentrated solution such as a melt or a gel. On a typical logarithmic plot of electrophoretic mobility vs. molecular size M, the biased reptation model is used to describe the linear region having a slope of -1.0. The curve then becomes concave for double-stranded DNA molecules larger than about 40 kbp in agarose gels (or for single-stranded DNA molecules larger than about 1kb in a polyacrylamide gel).

Recent experimental results from Calladine et al. [21] and Arvanitidou et al. [58] have shown that the gel electrophoretic mobility of the DNA molecules can decrease as fast as M^{-3} for small DNA sizes. The group of Mayer, Slater and Drouin has found a $M^{-1.6}$ [59] dependence for similarly small DNA molecules. These new and surprising results do not agree with the M^{-1} law predicted by the reptation model [51-53]. Zimm and Lumpkin (ZL) recently developed a new model to explain such behavior [19]. They modeled the electrophoresis of macro-ions in an irregular gel using a modified reptation theory and found that the mobility indeed decreases faster than M^{-1} for intermediate DNA molecules. They also showed that the dependence of the diffusion coefficient can change from being governed by a power law (predicted by the reptation

model) to an exponential in the zero field limit.

This chapter is organized as follows: Section 4.2 presents the reptation model; Section 4.3 describes the effect of an irregular matrix on the reptation model (the ZL model is described in this section as well as our new approach); Section 4.4 gives a stochastic description of the problem of the diffusion of a particle between two absorbing walls; Section 4.5 describes the computer simulation which we used to study the dynamics of a reptating DNA molecule in an irregular matrix. Our findings are then discussed in Section 4.6 and we conclude in Section 4.7.

4.2 The Reptation Model

4.2.1 The Tube and the Reptation Model

The gel in which electrophoresis is carried out may be seen as a cage for the migrating polymer (or probe). The three-dimensional lattice formed by the gel fibers constitutes a set of topological constraints [49] that cannot be crossed by the probe (Fig. 4.1a). We can thus represent the macromolecule inside an imaginary tube [49,60-63] as shown in Fig. 4.1b. It can

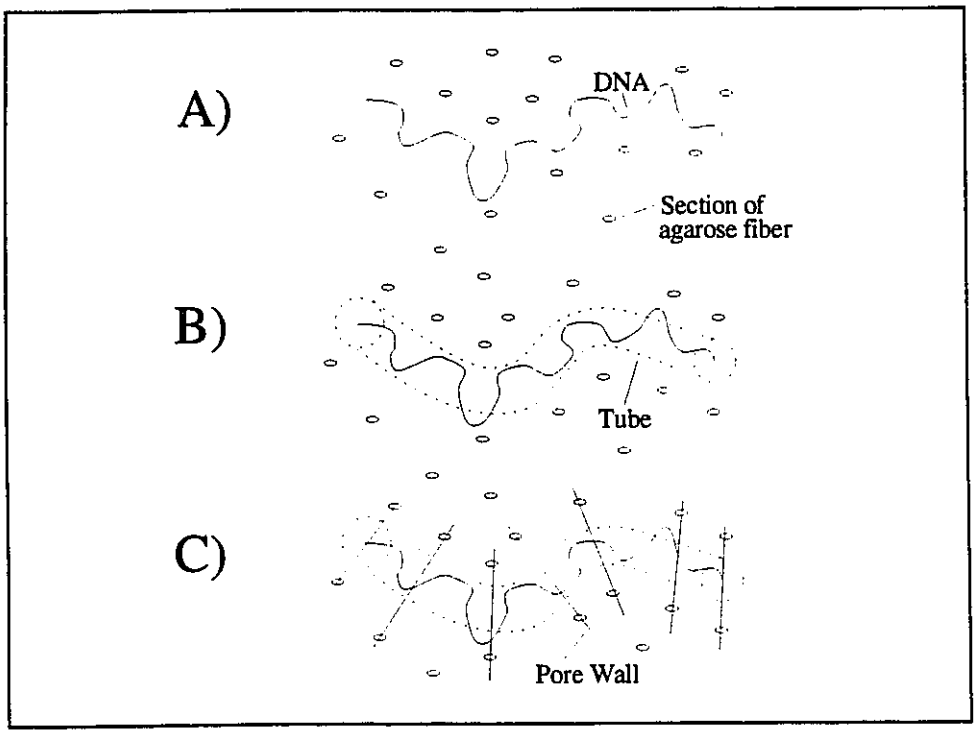

Figure 4.1 Representation of the Tube in the Reptation Model

be seen that the conformation of the polymer is almost confined to a tube-like region assuming that the probe (polymer) is much longer than the interfiber spaces. According to the reptation theory, the polymer is modeled as a "primitive" chain of N effective "reptation segments" which is assumed to be confined tightly to this random-walk tube (the polymer is not being allowed to bend away from the tube axis). This tube is embedded in the gel matrix of cross-linked chains, so that the macromolecule can move only along the axis of the tube (Fig. 4.1c).

4.2.2 The Dynamics of the Chain in the Reptation Model

In the absence of an electric field, the motion of the polymer is due solely to random thermal motion. The dynamics of the primitive chain in the reptation model are characterized by the two following assumptions:

a) The primitive chain and the tube have a constant contour length.

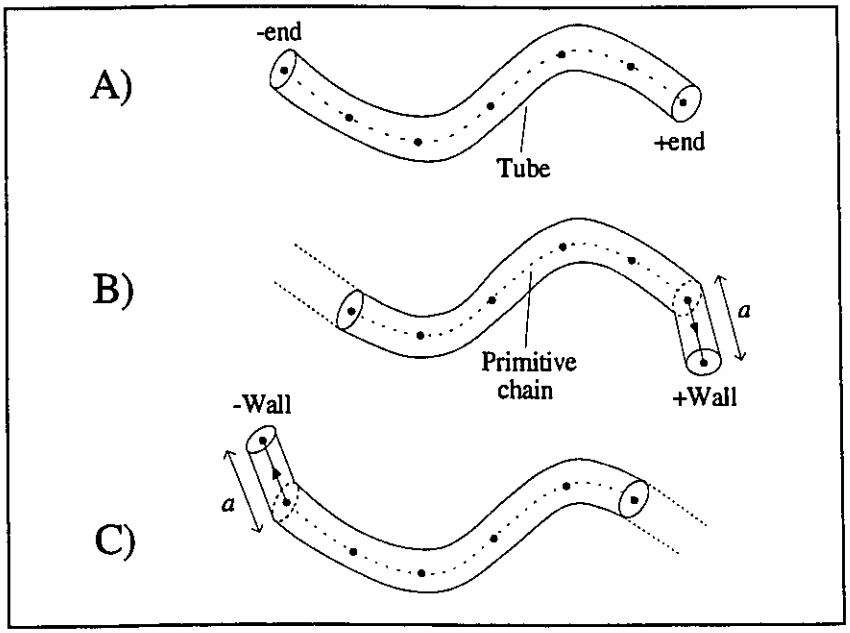

Figure 4.2 The Motion of the Chain in the Reptation Model
The first (last) segment is denoted +end (-end); the sign thus identifies the tube end. When the +end segment (-end segment) leaves the initial tube and goes towards the +Wall (-Wall) direction, a new tube section is created, while the -end segment (+end segment) follows the initial tube. Each jump is over the distance of a mean pore size *a*. This figure is adapted from Fig. 3.2 of ref. [66].

b) The only allowed motion for a primitive chain is along the tube axis.

Thus, the motion of the primitive chain is represented by a series of discrete displacements or "jumps" of the chain over the distance of a mean pore size a (Fig. 4.2). A pore is defined as a free volume element between two walls, each wall being roughly delimited by at least three fibers through which a polymer can move (Fig. 4.1c). A jump by the chain towards either end of the tube is equally probable due to the randomness induced by the thermal fluctuations (each jump takes a mean time τ_B).

The presence of an electric field parallel to the Cartesian coordinate x leads to a net force acting on the polyelectrolyte chain along its tube axis (the transverse components of this force play no role because of assumption `b` above). The duration and the probability of a "jump" in this situation can be obtained by comparing the displacement of the chain in the tube to the diffusion of a particle between two absorbing walls (Fig. 4.3) [64, 65]. A discrete jump of the chain thus corresponds to the motion of a particle that is absorbed at the end of a displacement of length a. In other words, the chain moves in its tube in response to Brownian motion (with a curvilinear diffusion constant D_c) and to the field-induced drift force by "jumping" over a distance equal to the mean pore size a. In the same way, the particle is subjected to an identical drift force as well as to thermal fluctuations expressed by the diffusion constant D_c.

The probabilities of jumping towards the $\pm$end of the tube (the + and − ends are defined arbitrarily) are given by [66]:

$$p_{\pm}(h_x) = \frac{1}{1 + \exp(\mp 2\delta)} \qquad (4.1)$$

where h_x is the end-to-end distance of the tube in the electric field direction, and the bias factor δ is defined as

$$\delta = \epsilon \frac{h_x}{a} \qquad (4.2)$$

with ϵ being the dimensionless measure of the field strength, also called the scaled electric field.

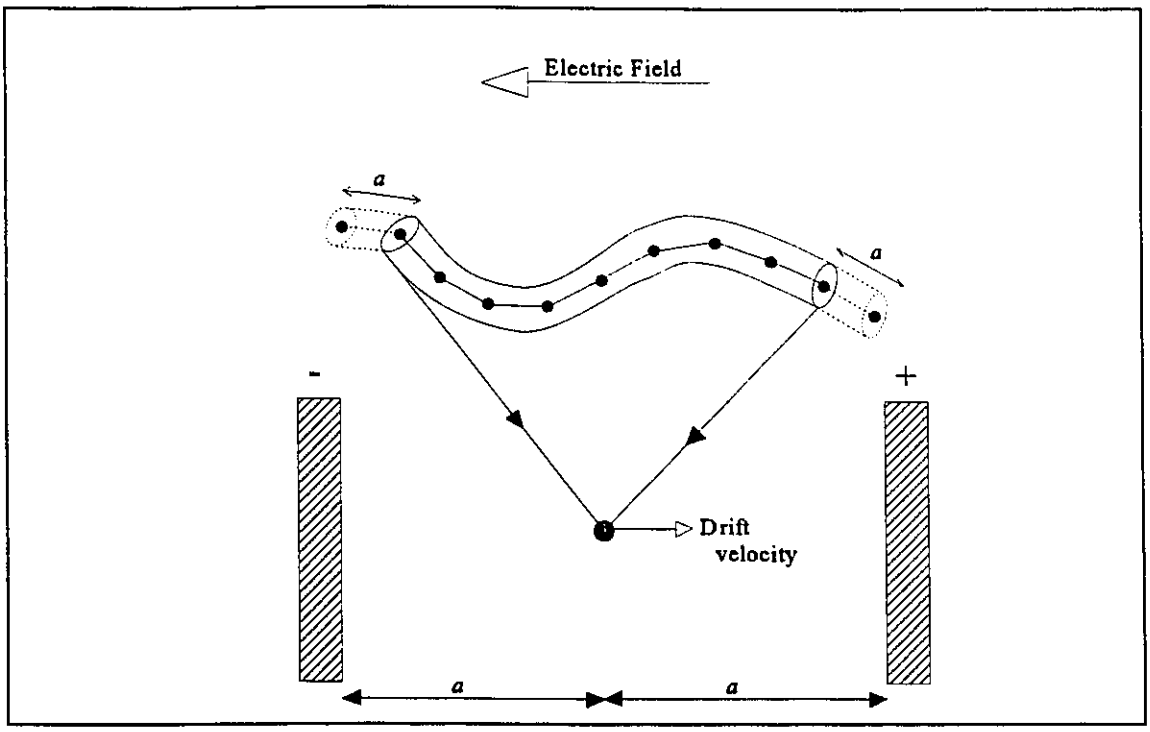

Figure 4.3 Analogy between the Chain and a Particle

The discrete motion of the chain in a uniform gel corresponds to the first passage problem of a moving particle between two absorbing walls. When the chain jumps over the length of a pore of size a, the particle is absorbed by one of the two walls at the end of the displacement (of length a). Thus, if the polymer displacement is towards the +end segment (-end segment), the particle will jumps towards the +Wall (-Wall). The longitudinal field-induced drift velocity of the chain is the same as the drift velocity of the particle; the chain length is collapsed on the particle since the chain is assumed to move coherently. This figure is adapted from Fig. 3.3 of ref. [66].

This parameter is defined as

$$\epsilon = \frac{qEa}{2k_BT} \tag{4.3}$$

where (qE) is the electric force acting on one reptation segment and (k_BT) is the thermal energy. The average first-passage time required to jump over a distance a (in either direction) is given by [66]

$$\tau(h_x) = \frac{\tanh(\delta)}{\delta} \cdot \tau_B \tag{4.4}$$

where $\tau_B = a^2/2D_c$ is defined as the Brownian time necessary for the diffusion of the chain over a curvilinear distance $\langle a^2 \rangle^{1/2}$ when $\epsilon = 0$. The probability that the new (jumping) end-segment will assume an orientation $\Theta(t)$ $(0 \leq \Theta \leq \pi)$ with the field axis is [67]

$$P(\Theta)d\Theta = \frac{1}{2} \frac{\epsilon}{\sinh(\epsilon)} \sin(\Theta)d\Theta \; e^{\epsilon \cos(\Theta)} \qquad (4.5)$$

We note that if the field is turned off ($\epsilon = 0$), $P(\Theta)d\Theta = 1/2 \sin(\Theta)d\Theta$ as expected [68]. Using these equations, we can model DNA gel electrophoresis (for $\epsilon > 0$) or normal reptation (for $\epsilon = 0$) using computer simulations or analytical calculations.

4.3 The Effect of an Irregular Matrix

4.3.1 Introduction

In the reptation theory, each pore of the gel is assumed to be energetically equivalent [14,18]. This assumption is probably not valid for various reasons. For instance, if the polymer moves in a narrow, curved space, either the macromolecule must bend or the gel must deform or both. Each of these cases requires energy and can lead to local energetic effects. Also, one may even have direct interactions between the fibers and the segments of the polymer. The effect of these deformations or interactions on the dynamics of the system can be very significant (e.g., it may change the scaling laws [19]). In this Section, I will first introduce the ZL model for the reptation of a polymer chain in an irregular matrix [19] and I will show the results obtained by Zimm and Lumpkin. I will then describe a new model that we developed and compare its results with those of Zimm and Lumpkin [19].

4.3.2 Elements of the ZL Model

To model the electrophoresis of polyelectrolytes in an irregular matrix, Zimm and Lumpkin simply add a free energy term to the familiar tight-tube reptation model. As mentioned, the polymer molecule is made of N rigid segments confined to a random-walk tube. The curvilinear axial coordinate of that tube is called the 's' coordinate, and we set the electric field to be parallel to the x-axis (in Cartesian coordinates). In the irregular matrix, each segment of the probe interacts with the environment with a given energy. This energy fluctuates with the

s-coordinate of the segment as the segment moves along 's', that is, along the tube axis. In other words, the energy of the segment remains fixed as long as the segment occupies a given pore. When the segment leaves this pore, the energy of that segment changes. This hypothesis is probably appropriate for a cross-linked network such as a gel. Since the energy of the segments changes when the polymer moves, the total free energy of the molecule is a random variable (with some memory due to the slow process of tube renewal [49]).

Zimm and Lumpkin simplified the dynamics of the chain by assuming that each "jump" was over a curvilinear length Na (i.e., each jump totally renews the tube). Reptation models are generally studied using discrete "jumps" of length a which introduce complicated memory effects. We believe that ZL's approximation can lead to severe artifacts because of the loss of the memory effects which are normally present in reptation models.

The average of the x-component of the chain velocity is expressed in terms of the curvilinear current J of the system and the concentration C_x at that point:

$$\langle \dot{x} \rangle = \frac{\int_0^x dx'}{\int_0^t dt'} = \frac{x\,J}{\int_0^x C_x(x')\,dx'} \tag{4.6}$$

where x is the total distance traveled by the DNA molecule. We can simplify by defining a reduced concentration W as

$$W = \frac{D_c\,C_x}{J} \tag{4.7}$$

Thus the relative, time-averaged velocity found by ZL can be expressed as

$$\frac{\langle \dot{x} \rangle}{\langle \dot{x}_0 \rangle} = \frac{x}{(NqE/k_BT)\int_0^x W(x')\,dx'} \tag{4.8}$$

The reference velocity, also called the free-drift velocity of the DNA, is defined as

$$\langle \dot{x}_0 \rangle = qE/\xi = D_c NqE/k_B T \tag{4.9}$$

where ξ is the friction coefficient of a DNA primitive segment. To solve Eq. (4.8), one must first obtain the reduced concentration by integrating the following relation

$$\frac{dW}{dx} + W\frac{d\Psi}{dx} = -\frac{1}{P} \tag{4.10}$$

(this expression comes directly from the one-dimensional diffusion equation with an external-force term) where

$$P = \left(\frac{dx}{ds}\right)^2 = \left(\frac{h_x}{L}\right)^2 \tag{4.11}$$

is the projection factor and

$$\Psi = (-NqEx + G)/k_B T \tag{4.12}$$

is the reduced free energy. Here, $L=Na$ is the contour length of the primitive chain and G is a fluctuating free energy term. Zimm and Lumpkin solved this problem by integrating backward in the negative x direction. In other words, they selected a state at $x=0$ and integrated backwards to see what value of x (negative) led to it. They assumed that neither Ψ nor P vary significantly over a distance δx, with $|\delta x| \leq |h_x|$. If Ψ and P can be approximated as constants, we can integrate Eq. (4.10) analytically. Thus, Zimm et Lumpkin found that the integration of the reduced concentration W can be expressed as

$$\int_0^{\delta x} W(x)\, dx = \frac{\delta x}{FP} + \frac{1/FP - W_i}{F}\left[1 - \exp(F\,\delta x)\right] \tag{4.13}$$

where W_i is the value of W at the beginning of the interval and

$$F = -d\Psi/dx \tag{4.14}$$

is the reduced force. In most of their work, Zimm and Lumpkin take $\delta x = -|h_x|$ (this corresponds to a very large integration step as discussed before). To integrate over a large interval, they divide this interval into small steps δx taking the final W of each step as the initial value W_i of the following step. The total integration is simply the sum of these small steps. But to carry out these integrations, one must also calculate the force F and the projection factor P.

The force F is the derivative of Eq. (4.12) which is the sum of two terms, one coming from the effect of the electric field and the other from the local random free energies. The local free energy term G is assumed to be the sum of the free energies g_i of the segments. ZL assumed that the g_i's follow a distribution $w(g_i)$ with a mean value

$$m = \int g_i w(g_i)\, dg_i \tag{4.15}$$

and, a variance

$$g^2 = \int (g_i - m)^2 w(g_i)\, dg_i \tag{4.16}$$

where m and g are adjustable parameters. These authors further assumed that there is no correlation between the values g_i for consecutive segments, meaning that the correlation length of the matrix is shorter than the segment length *a* of the primitive chain.

From the central limit theorem, we know that if the number of segments N is very large, the probability distribution function for G follows a Gaussian distribution

$$w(G) = \frac{1}{\sqrt{2\pi N g^2}} \exp\left[-\frac{(G-Nm)^2}{2Ng^2}\right] \tag{4.17}$$

with a mean Nm and a standard deviation $N^{1/2}$ g. If the number of segments N is small, G is simply the sum of the g_i of each segment. In this case, the distribution used by ZL satisfying Eqs.

(4.15) and (4.16) is

$$w(g_i) = \exp(-g_i/g)/g \tag{4.18}$$

with $g_i \geq 0$. The local free energy contribution to the force F is assumed to be the difference between the local energies G of the two conformations (i.e. before and after the jump of size δx). One can then rewrite the force F as:

$$F = \frac{G_1 - G_2}{\delta x} + N a_D q E / k_B T \tag{4.19}$$

where G_1 and G_2 are the G values of the two conformations (in $k_B T$ units) and a_D is the Kuhn segment length (≈115 nm [69]). The a_D in the second term appears because we want all lengths, such as δx, to be dimensionless.

The energy model used by ZL is qualitatively equivalent to the barrier energy model (Fig. 4.4). However, the difference between the energy barrier and local energy models is very important. In the local energy model, the energy required for the displacement of the primitive chain is simply the difference in energy between the new tube section that is created and the old tube section that is destroyed after the jump (Fig. 4.2). In the energy barrier model, the energy required for the displacement of the polymer is the sum of all the local energies g_i. One can see that the barrier model requires much more energy for the displacement of the molecule than the local energy model. This leads to very different results. Since ZL used $\delta x = h_x$, it is more appropriate to define their model as an energy barrier model instead of a local energy model.

To calculate the projection factor P needed for Eq. (4.13), we must know the x-component of the end-to-end distance, h_x, of the polymer. This value is obtained from a table of frequencies. The frequencies are directly proportional to the probability of occurrence $p(h_x)$ of the different values of h_x [70]. Note that ZL did not take the effect of the energy fluctuations into account in this table; this ignores the well-known memory effects that characterize the reptation models.

With the definitions given in this section, ZL were able to obtain a first model of DNA electrophoresis inside an irregular matrix [19]. Figure 4.5 shows the relative electrophoretic mobility versus the inverse of the length of the polymer for $g=0$. From Fig. 4.5, one can see that

the ZL model (with g=0) agrees with the biased reptation theory [51-52]. Figure 4.6 shows the relative mobility versus the length of the probe for g=0.5 k_BT. The effect of free energies is negligible for high electric fields and large values of N; but for low field intensities, the relative mobility decreases significantly for intermediate values of N. This decrease is due to the local traps created by the random fluctuations of the local energies.

The relation found by ZL for the relative diffusion coefficient in the zero field limit is given by

$$\frac{D_x}{D_0} = \lim_{E \to 0} \frac{\langle \dot{x} \rangle}{\langle \dot{x}_0 \rangle} = \frac{(Ng^2)^2 e^{-Ng^2}}{4} \left(1 - \frac{4}{Ng^2} + \ldots \right) \qquad (4.20)$$

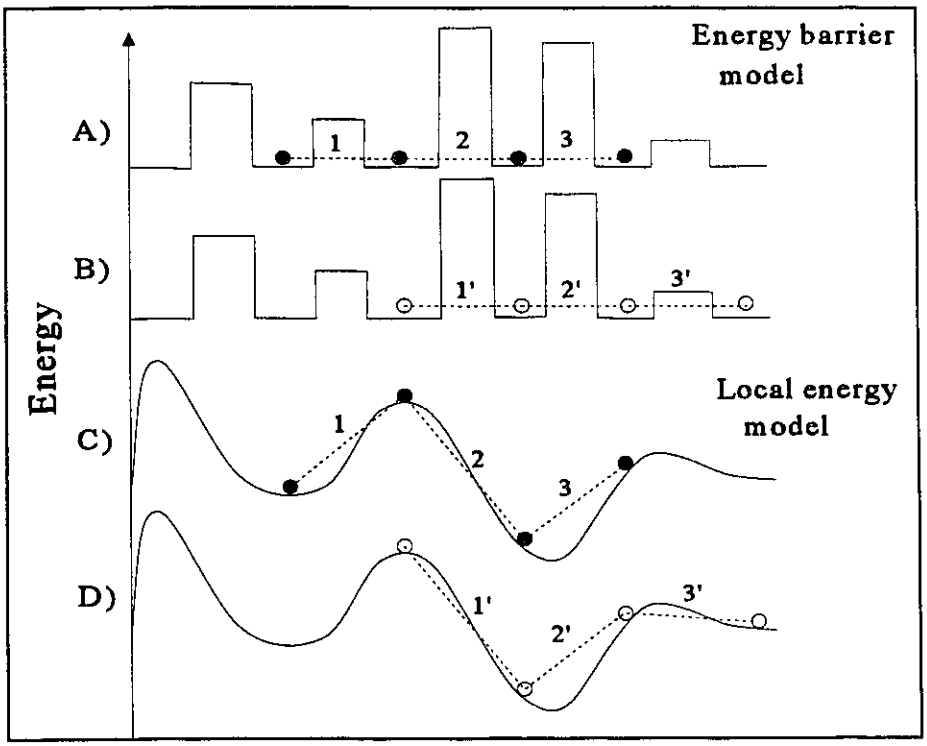

Figure 4.4 The Energy Barrier and Local Energy Models
Schematic illustration of the difference between the local free energy model and the energy barrier model. The total energy cost in the former model is much lower than in the latter; in the barrier model, the energy required for the displacement of the chain (from (A) to (B)) is the sum of the energy barriers whereas in the local free energy model, the total energy required for the displacement (from (C) to (D)) is the difference in energy between segments 1 and 3'.

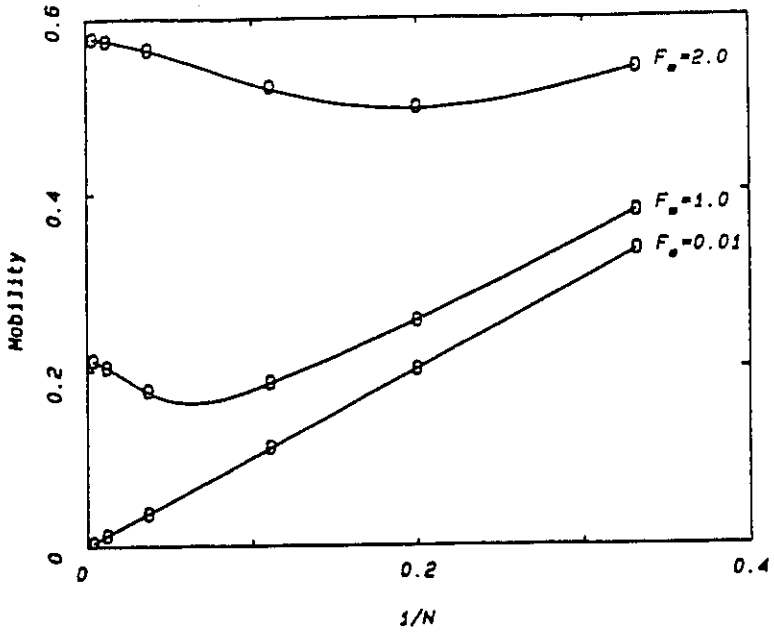

Figure 4.5 Electrophoretic Mobility vs. 1/N for g = 0
The curves indicate the mobility calculated from the reptation theory and the points indicate the mobility calculated by the ZL method. The parameter F_e which is directly proportional to ϵ is equal to $a_D qE/k_B T$ (second term of Eq. (4.19) divided by N). This is Fig. 1 of ref. [19].

where D_x is the x-component of the diffusion coefficient. For very large values of N, the dependence of the relative diffusion coefficient upon the molecular size N is exponential. Figure 4.7 shows the zero-field relative diffusion coefficient versus the length of the polymer for three different values of g: 0, 0.1, and 0.5. The diffusion coefficient decreases substantially when g is increased or the length of the probe N is increased.

In conclusion, ZL found that the interactions between the probe and the gel can decrease the mobility as well as the zero-field diffusion coefficient. In the case of the mobility, the effects of trapping are strongest for intermediate polymer sizes. This is due to the different contributions from the free energy G and the field E (see Eq. (4.19)). We have noted that the root-mean-square fluctuation of G (standard deviation) increases as $N^{1/2}$ (first part of Eq. (4.19)). On the other hand, the electric forces increase as the first power of the length of the polymer N (second part of Eq. (4.19)). Thus, for short polymers, the values of G are too small to create effective traps,

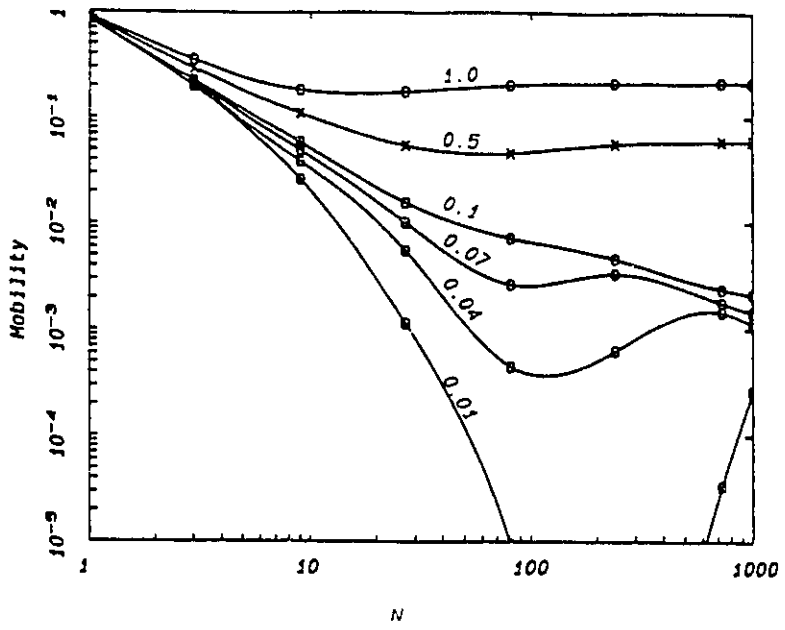

Figure 4.6 Electrophoretic Mobility vs. N for g = 0.5
The numbers on the curves give the value of F_e (see Fig. 4.5). The points are calculated using the ZL model; the curves are cubic-spline interpolations. Some points of the F_e=0.01 calculation are outside the visible plotting area. This is Fig. 3 of ref. [19].

while for large values of N, the electric forces easily overwhelm the free energy. Thus it is only for the intermediate values of N that G is of any importance. For the diffusion coefficient, we have seen that D_x decreases when g or N is increased. This reduction of the diffusion coefficient was found by Muthukumar and Baumgartner [71, 72] in their model of entropic barriers. It would have been interesting to observe the behaviour of the diffusion coefficient for different values of g when an electric field is applied to the system; however, such a comparison has not been done by ZL or by any other group.

4.3.3 A New Model

Our model also uses a modified reptation theory [51-53] with local free energies to explain the behaviour of polymers inside an irregular matrix. We assume that the energy associated with a given pore remains fixed as long as a segment occupies this pore. This assumption is probably

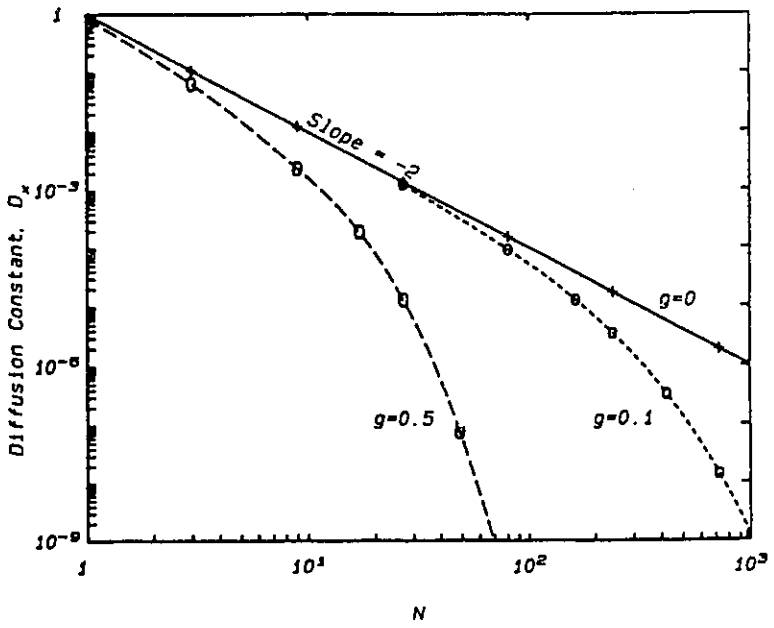

Figure 4.7 Log-Log Plot of the Diffusion Coefficient vs. N
D_x is calculated in the low-field limit as a function of N. This is Fig. 8 of ref. [19].

valid for a stiff gel. We further assume that the correlation length of the matrix is shorter than the segment length of the probe so that there is no correlation between the various g_i`s (g_i is defined as the free energy of segment i). The distribution function $w(g_i)$ used for g_i is a gaussian function with a mean m = 0 and a standard deviation g such that Eqs. (4.15) and (4.16) are satisfied,

$$w(g_i) = \frac{1}{\sqrt{2\pi g^2}} \exp\left[-\frac{g_i^2}{2g^2}\right] \tag{4.21}$$

In practice, we cut the gaussian beyond 2g in order to avoid exceedingly large trapping times.

As described previously, the displacement of the chain inside the tube can be represented as the diffusion of a particle between two absorbing walls [64, 65]. Figure 4.3 gives a schematic description of this analogy. The one-dimensional space of the particle problem is equivalent to

the curvilinear tube axis (not the field axis). Thus, when the particle is absorbed by the + (or −) wall, we say that the chain has successfully completed a jump towards the + (or −) end of its entanglement tube. The effect of the electric field is replaced by a drift velocity v_e which can be obtained from a scaled potential function U, i.e. $v_e = -\nabla U$. Figure 4.8 shows a uniform electric field (no energy fluctuation) where $U_\pm$ ($= \mp 2\delta D_c$) is simply the value of the potential at the $\pm$wall and $x_\pm$ ($= \pm a$) is the position of the $\pm$wall given that the particle is at the origin (x=0) before the jump. The potential function U(x) is thus given by

$$U(x) = -\frac{2\delta D_c}{a} x \qquad (4.22)$$

From the above equation, one can see that the drift velocity v_e is simply the slope of the curve

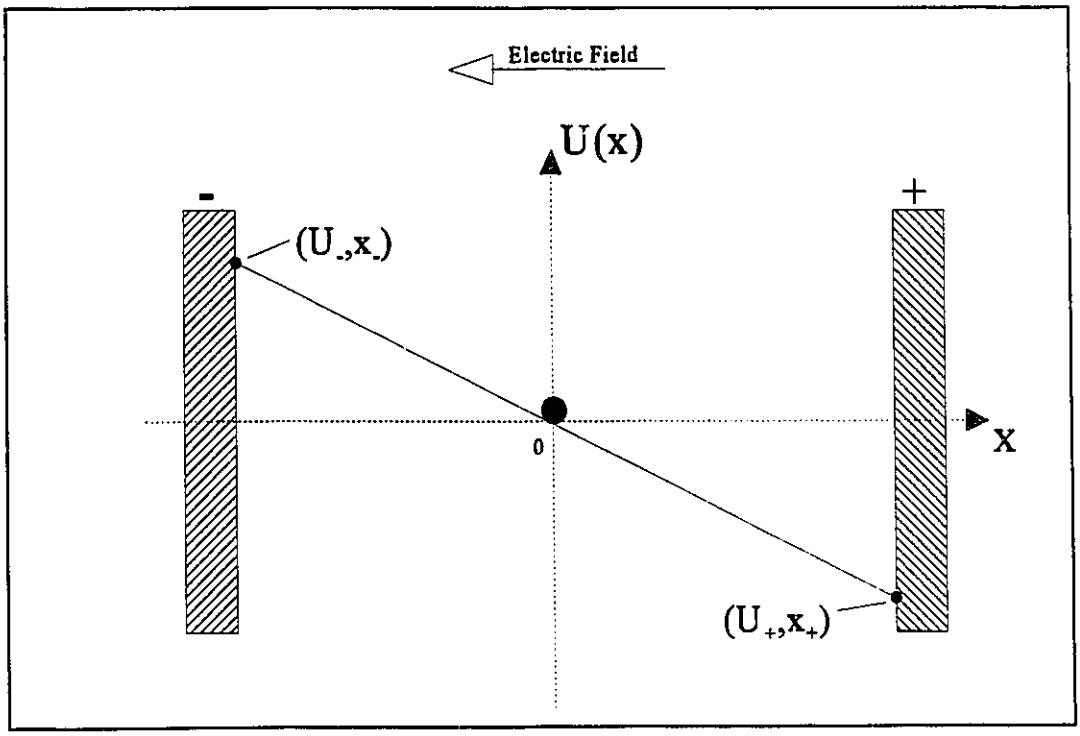

Figure 4.8 Particle in a Uniform Electric Field
Illustration of the analogy of the particle in a uniform electric field. The value of the potential at the $\pm$wall is given as $U_\pm = \mp 2\delta D_c$ whereas the value of the position is given by $_\pm x = \pm a$. Knowing that the particle is initially at the origin (x=0), one can easily calculate the drift velocity v_e from the potential function.

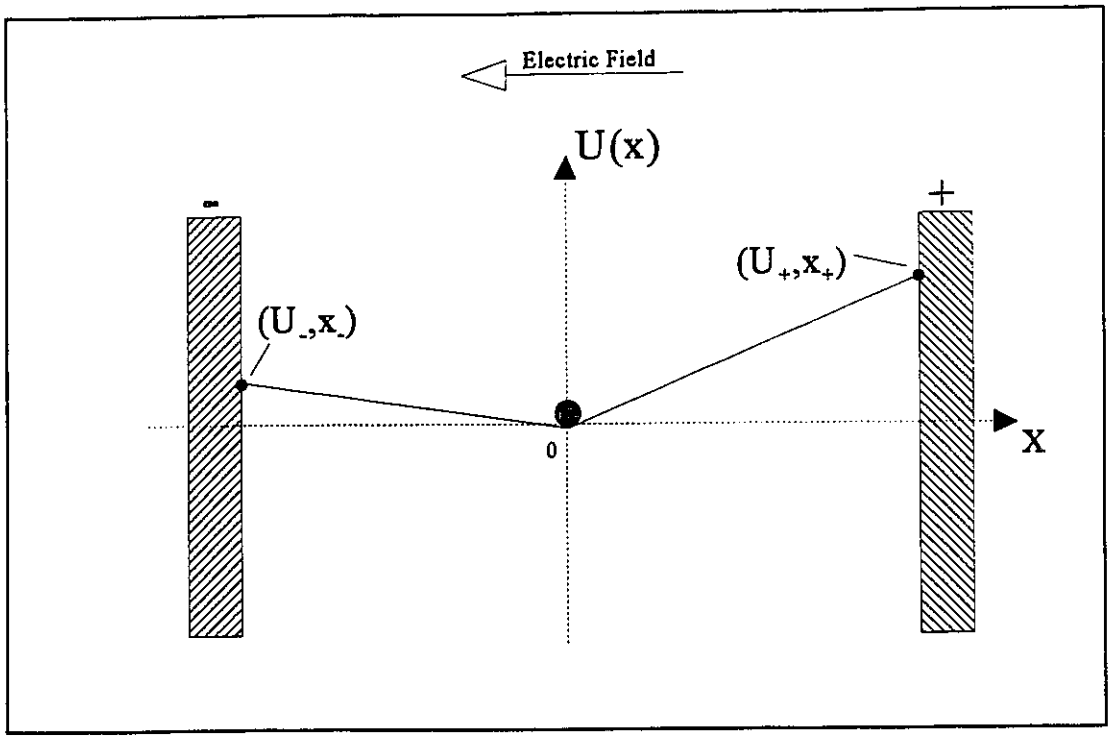

Figure 4.9 Particle in Uniform Electric Field with Random Energy Fluctuations
Illustration of the analogy of the particle in a uniform electric field with local free energy fluctuations. The value of the potential at the ±wall is given as $U_\pm$ and the value of the position is given by $x_\pm = \pm a$. In this problem, the drift velocity depends on the direction of the jump. If the jump is toward the +wall, the drift velocity v_{+e} is given by U_+/x_+ (which is different than U_-/x_-) and if the jump is towards the -wall, the drift velocity v_{-e} is simply U_-/x_-.

represented in Fig. 4.8.

We will now investigate the effect of an irregular matrix on the reptation dynamics. Note that in our model, the polymer jumps over a curvilinear distance equal to the size of a pore ($\delta x \leq a$); we do not use $\delta x \approx h_x$ as ZL do. For a constant electric field, the effect of the local free energies is represented as a random perturbation of the potentials $U_\pm$ (Fig. 4.9). These new values of U are simply the sum of two terms: the potential due to the constant electric field ($\mp 2\delta D_c$) and the random energy term,

$$U_\pm = \mp 2\delta D_c + \left(g_{\pm wall} - g_{\mp end}\right) \qquad (4.23)$$

where $g_{\pm wall}$ is the value of g_i at the ±wall and $g_{\mp end}$ is the value of g_i for the ∓end segment of the

probe. This relation is similar to equation Eq. (4.19) derived by ZL. Thus, when the chain slides over a curvilinear distance a in the $\pm$ direction, the $\mp$end segment (with an energy $g_{\mp end}$) disappears while a new tube segment (with an energy $g_{\pm wall}$) is created at the $\pm$end of the tube. Since all the internal chain segments simply slide, there is no net change in energy elsewhere along the chain. In this sense, our model is unlike a "barrier model" where each segment must overcome a local potential barrier for the chain to jump as a whole.

The mean first-passage time and the probability that the particle will jump towards a particular wall can be derived using stochastic methods (more precisely, the Fokker-Planckequation). We also calculate the second moment of the passage time to evaluate the diffusion coefficient of the polymer during the electrophoresis process. With these expressions, one can describe the details of the motion of the DNA inside an irregular matrix during electrophoresis, or in absence of an electric field, by using computer simulations. We feel that this new approach is more reliable since we use $\delta x \leq a$ as in the usual reptation models; it also allows us to study the electric field dependence of the diffusion constant.

4.4 Stochastic Methods*

4.4.1 The Chapman-Kolmogorov Differential Equations

The Chapman-Kolmogorov equation for the transition density $p(x_1,t_1|x_3,t_3)$ of a Markov process can be expressed as

$$p(x_1,t_1|x_3,t_3) = \int dx_2\ p(x_1,t_1|x_2,t_2)p(x_2,t_2|x_3,t_3) \qquad \textbf{(4.24)}$$

This results from the general definition of a Markov random sequence in which there exists a one step density that would sequentially yield the same results. In other words, the probability that a particle will be at x_1 at a time t_1, knowing that it was previously at x_3 at a time t_3 is equal to the sum of the product of 1) the probability that it will be at x_1 at a time t_1 knowing that it will pass by x_2 at a time t_2 and 2) the probability that the particle will be at x_2 at a time t_2 knowing that

---

* This Section is inspired from: Gardiner, C.W.: *HandBook of Stochastic Methods* (Springer-Verlag, Berlin, Heidelberg 1983).

it was previously at x_3 at a time t_3. The solution of the Chapman-Kolmogorov equation is easier to obtain from its differential form. This differential equation does not seem to have any agreed upon name in the literature. I will call it the differential Chapman-Kolmogorov equation (DCKE). Its general form, for a one-dimensional situation, reads

$$\begin{aligned} \partial_t\, p(x,t|x',t') &= -\frac{\partial}{\partial x}[A(x,t)p(x,t|x',t')] \\ &+ \frac{1}{2}\frac{\partial^2}{\partial x^2}[B(x,t)p(x,t|x',t')] \\ &+ \int dy\, [W(x|y,t)p(y,t|x',t') - W(y|x,t)p(x,t|x',t')] \end{aligned} \tag{4.25}$$

where $p(x,t|x',t')$ is the conditional probability density that a particle will be at position x at time t knowing that it was at position x' at a previous time t', A(x,t) is the drift velocity, B(x,t) is the diffusion coefficient and $W(x|x',t)$, the distribution function is defined as follows

$$W(x|x',t) = \lim_{\Delta t \to 0} p(x,t+\Delta t|x',t)/\Delta t \tag{4.26}$$

The distribution function W is simply a rate of transition probability. The initial condition that the DCKE has to satisfy is

$$p(x,t|x',t) = \delta(x-x') \qquad \forall\ t \tag{4.27}$$

which follows from the definition of the conditional probability density. If we assume $W(x|x',t)$ to be zero (no discontinuous jump process), the DCKE reduces to the Fokker-Planck equation (FPE):

$$\partial_t\, p(x,t|x',t') = -\frac{\partial}{\partial x}[A(x,t)p(x,t|x',t')] + \frac{1}{2}\frac{\partial^2}{\partial x^2}[B(x,t)p(x,t|x',t')] \tag{4.28}$$

The corresponding process is known mathematically as a diffusion process. One can also derive the backward differential Chapman-Kolmogorov equation from the Chapman-Kolmogorov equation (with $W(x|x',t') = 0$):

$$\partial_{t'} p(x,t|x',t') = - A(x',t')\frac{\partial p(x,t|x',t')}{\partial x'} - \frac{1}{2} B(x',t')\frac{\partial^2 p(x,t|x',t')}{\partial x'^2} \qquad (4.29)$$

Since the forward and backward equations are equivalent, they are both useful. The appropriate initial condition for both equations is given by Eq. (4.27). The forward equation gives directly the values of the measurable quantities as a function of time t and tends to be used more commonly in applications. The backward equation is more useful in the study of first-passage times or exit problems, in which cases we use this equation to find the probability that a particle leaves a certain region in a given time.

4.4.2 The Fokker-Planck Equation

We can rewrite Eq. (4.28) in the following way,

$$\partial_t p(x,t|x',t') + \partial_x J(x,t|x',t') = 0 \qquad (4.30)$$

with the initial condition,

$$p(x,t'|x',t') = \delta(x-x') \qquad (4.31)$$

where we define the probability current $J(x,t|x',t')$ as follows

$$J(x,t|x',t') = A(x,t)p(x,t|x',t') - \frac{1}{2}\partial_x[B(x,t)p(x,t|x',t')] \qquad (4.32)$$

For a homogeneous process, the drift and the diffusion coefficient are time independent. In such a case, we rewrite the above expression as:

$$J(x,t|x',t') = A(x)p(x,t|x',t') - \frac{1}{2}\partial_x[B(x)p(x,t|x',t')] \qquad (4.33)$$

4.4.3 The Mean Exit Time (for the interval [a,b])

The total probability that the particle exits through x=a after time t is given by the time

integral of the probability current at x=a. We thus define this probability by (with a≤x≤b)

$$\begin{aligned} p_a(x,t) &= -\int_t^\infty dt'\, J(a,t'|x,0) \\ &= \int_t^\infty dt' \left\{ -A(a)p(a,t'|x,0) + \frac{1}{2}\partial_a[B(a)p(a,t'|x,0)] \right\} \end{aligned} \tag{4.34}$$

where the negative sign is needed to point the current to the left. We also have

$$p_b(x,t) = \int_t^\infty dt' \left\{ A(b)p(b,t'|x,0) - \frac{1}{2}\partial_b[B(b)p(b,t'|x,0)] \right\} \tag{4.35}$$

for the probability that the particle exits through x=b after time t. The probability that the particle exits at a time $T_a > t$, given that it exits through x=a, is

$$\text{Prob}(T_a > t) = p_a(x,t)/p_a(x,0) \tag{4.36}$$

Since the system is time-homogeneous, we can write

$$p(a,t|x,0) = p(a,0|x,-t) \tag{4.37}$$

Using the fact that p(a,t|x,0) satisfies a backward FPE, we have

$$\begin{aligned} A(x)\partial_x p_a(x,t) + \frac{1}{2}B(x)\partial_x^2 p_a(x,t) &= -\int_t^\infty dt'\, \partial_t J(a,t'|x,0) \\ &= J(a,t|x,0) = \partial_t p_a(x,t) \end{aligned} \tag{4.38}$$

If G(x,t) is the probability that T≥t, the mean of any function of T is calculated as

$$\langle f(T) \rangle = -\int_0^\infty f(t)dG(x,t) \tag{4.39}$$

Thus the mean exit time, given that the exit is through x=a, is

$$T(a,x) = -\int_0^\infty t\, \partial_t \mathrm{Prob}(T_a > t)dt = \int_0^\infty p_a(x,t)dt / p_a(x,0) \tag{4.40}$$

Integrating Eq. (4.38) with respect to t from 0 to ∞ results in

$$A(x)\partial_x[p_a(x)T(a,x)] + \frac{1}{2}B(x)\partial_x^2[p_a(x)T(a,x)] = -p_a(x) \tag{4.41}$$

where we defined

$$p_a(x) = \text{probability of exit through } a = p_a(x,0) \tag{4.42}$$

The boundary conditions for this equation are quite straightforward since they follow from those for the backward FPE, namely,

$$p_a(a)T(a,a) = p_a(b)T(a,b) = 0 \tag{4.43}$$

In the first term, T(a,a) is zero (the time to reach a from a is zero) while in the second term, $p_a(b)$ is zero (the probability of exiting through a, when starting from b, is zero). One can then solve Eq. (4.41) for the mean exit time, given that the particle exits through x=a,

$$T(a,y) = 2\left[\frac{1}{p_a(y)}\int_y^b \frac{dx}{\psi(x)}\int_a^x \frac{dx'\psi(x')p_a(x')}{B(x')} - \int_a^b \frac{dx}{\psi(x)}\int_a^x \frac{dx'\psi(x')p_a(x')}{B(x')}\right] \tag{4.44}$$

or, doing the same calculation, one could find the mean exit time, given that the particle exits through x=b:

$$T(b,y) = 2\left[\int_a^b \frac{dx}{\psi(x)}\int_a^x \frac{dx'\psi(x')p_b(x')}{B(x')} - \frac{1}{p_b(y)}\int_a^y \frac{dx}{\psi(x)}\int_a^x \frac{dx'\psi(x')p_b(x')}{B(x')}\right] \tag{4.45}$$

where $\Psi(x)$ is defined as

$$\psi(x) = \exp\left\{ \int_a^x dx' \frac{2A(x')}{B(x')} \right\} \tag{4.46}$$

4.4.4 The Second Moment for the Exit Time

The second moment for the exit time, given that the particle exits through x=a, is

$$T^2(a,x) = -\int_0^\infty t^2\, \partial_t \mathrm{Prob}(T_a > t)dt = 2\int_0^\infty t\; p_a(x,t)dt/p_a(x,0) \tag{4.47}$$

We can derive an equation for $T^2(a,x)$ from Eq. (4.38):

$$A(x)\partial_x[p_a(x)T^2(a,x)] + \frac{1}{2}B(x)\partial_x^2[p_a(x)T^2(a,x)] = -2\; p_a(x)T(a,x) \tag{4.48}$$

One can solve for the second moment T^2 given that the exit is through x=a,

$$T^2(a,y) = 4\left[\frac{1}{p_a(y)} \int_y^b \frac{dx}{\psi(x)} \int_a^x \frac{dx' p_a(x')T(a,x')\psi(x')}{B(x')} - \int_a^b \frac{dx}{\psi(x)} \int_a^x \frac{dx' p_a(x')T(a,x')\psi(x')}{B(x')} \right] \tag{4.49}$$

One can also find T^2 given that the exit is through x=b,

$$T^2(b,y) = 4\left[\frac{-1}{p_b(y)} \int_a^y \frac{dx}{\psi(x)} \int_a^x \frac{dx' p_b(x')T(a,x')\psi(x')}{B(x')} + \int_a^b \frac{dx}{\psi(x)} \int_a^x \frac{dx' p_b(x')T(a,x')\psi(x')}{B(x')} \right] \tag{4.50}$$

4.4.5 The Probability of Exit

By letting t→0 in Eq. (4.38), we can see that $J(a,0|x,0)$ must vanish if $a \neq x$, since $p(a,0|x,0)=\delta(x-a)$. Hence, the right-hand side tends to zero and we get

$$A(x)\partial_x p_a(x) + \frac{1}{2}B(x)\partial_x^2 p_a(x) = 0 \tag{4.51}$$

with the following boundary conditions

$$\begin{aligned} p_a(a) &= 1 \\ p_a(b) &= 0 \end{aligned} \tag{4.52}$$

The solution of Eq.(4.51), given these boundary conditions and the normalization condition

$$p_a(x) + p_b(x) = 1 \tag{4.53}$$

is

$$p_a(x) = \frac{\int_x^b \frac{dy}{\psi(y)}}{\int_a^b \frac{dy}{\psi(y)}} \qquad p_b(x) = \frac{\int_a^x \frac{dy}{\psi(y)}}{\int_a^b \frac{dy}{\psi(y)}} \tag{4.54}$$

Using the above equations, together with those of Section 4.2.2, we can now model DNA electrophoresis in an irregular matrix.

4.5 Computer Simulations

4.5.1 The Algorithm

The equations derived in the previous section constitute the heart of our new model. In the case in which an irregular gel is used (Fig. 4.9), we can obtain the probability of jumping towards the ±end of the topological tube (or ±wall in our particle-between-walls analogy) from Eqs. (4.46) and (4.54),

$$p_{\pm} = \frac{\frac{|x_{\mp}|}{U_{\mp}}\left[e^{U_{\mp}/D_c} - 1\right]}{\frac{|x_{\pm}|}{U_{\pm}}\left[e^{U_{\pm}/D_c} - 1\right] + \frac{|x_{\mp}|}{U_{\mp}}\left[e^{U_{\mp}/D_c} - 1\right]} \tag{4.55}$$

where we have defined the drift coefficient (see Section 4.3.3) as

$$A(x) = \begin{cases} -U_-/x_- & , x \le 0 \\ -U_+/x_+ & , x \ge 0 \end{cases} \tag{4.56}$$

and the diffusion coefficient as

$$B(x) = 2D_c \tag{4.57}$$

The (huge) expressions for the first-passage time as well as the second moment of the first-passage time are given in Appendix A. We first need to verify that the new model reduces to the familiar tight-tube biased reptation model [51-53] when the effect of trapping is turned off (g=0). For the case of a uniform electric field (Fig. 4.3), we have $U_\pm = \mp 2\delta D_c$ and $x_\pm = \pm a$ (uniform pore size). With these values, we obtain the following expression:

$$p_\pm = \frac{1}{1 + e^{\mp 2\delta}} \tag{4.58}$$

for the probability of jumping, while the mean first-passage time is given by

$$t_\pm = \frac{\tanh(\delta)}{\delta}\,\tau_B \tag{4.59}$$

Therefore, we indeed recover Eqs. (4.1) and (4.4) from Section 4.2.2.

4.5.2 The Computer Program

A schematic diagram of the program used to simulate the electrophoretic migration of a chain in an irregular matrix is given in Fig. 4.10. The input and output data are displayed on the left and the processes are displayed on the right. The processes are divided into two groups: one for the generation of the chain, and the other for the motion of the chain.

The input parameters used in the simulation are 'seed', a seed number for the random number generator, 'N', the number of segments of the primitive chain, 'ϵ', the scaled electric field intensity, 'ensemb', the number of chains in the simulation (the size of the statistical ensemble; note that all the chains are run in parallel), and 'g', the standard deviation of the local energy

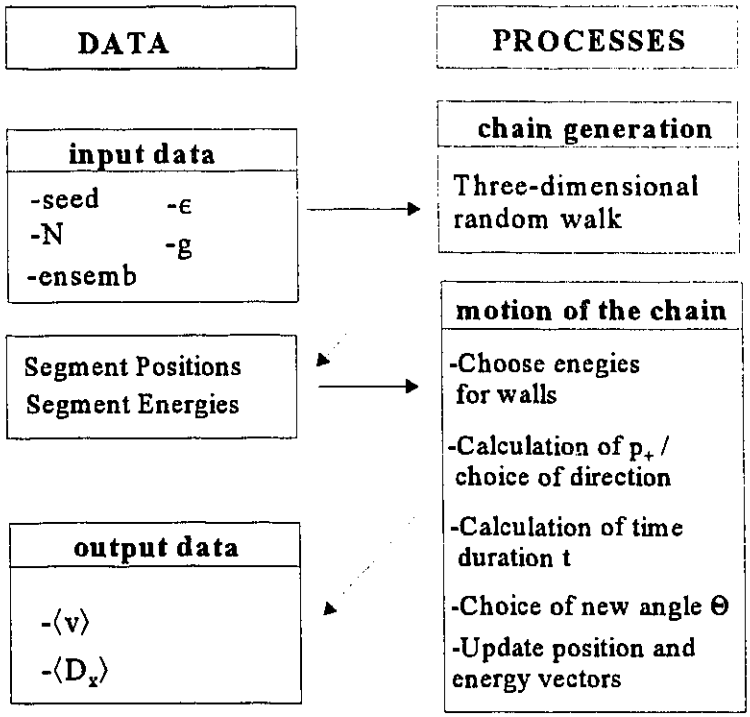

Figure 4.10 Schematic Diagram of the Computer Simulation

fluctuations. The output parameters obtained from the simulation are '⟨v⟩', the average electrophoretic velocity of the probe as a function of time, and '⟨D_x⟩', the average x-component of the diffusion coefficient as a function of time.

The initial conformation of the polymer is created by the chain generation process. Since the probe has a random conformation when loaded into the gel during a real electrophoresis experiment, the chain is created as a three-dimensional random walk where each step has a uniform length '*a*'. Note that an idealized freely-jointed primitive chain is used in the simulation to represent the DNA polymer; this implies that the length of the tube is assumed to be constant. An important aspect of this computer simulation is the absence of a predefined grid or lattice which would limit the chain motion to specific directions.

The continuous displacement of the probe in the irregular matrix is simulated by discrete jumps of length '*a*'. Thus, when the chain jumps, the leading end-segment creates a new tube section while the rest of the chain follows the initial tube. The orientation of the new tube section (in the case of polyelectrolytes and $\epsilon \neq 0$) is chosen according to the distribution of angles

Θ given by Eq.(4.5) [67]. The probability that the displacement of the probe will be towards the $\pm$end of the tube is given by relation (4.55), and the time duration of this displacement (of magnitude a) is given in Appendix A. Once the chain is created, with each segment having an energy g_i ($i=1,2...N$), the following procedure is used in the computer simulation for these discrete jumps:

- First, we calculate the end-to-end distance of the polymer, h_x,
- from which the bias parameter $\delta = h_x\epsilon/a$ is calculated. We need this parameter to calculate the potentials $U_\pm$.
- Next, the random energies of the two possible new tube sections $g_{\pm wall}$ are generated (following the truncated gaussian distribution function, Eq. (4.21)).
- With these values, we calculate $U_\pm$ (taking $x_\pm = \pm 1$ and $D_c = 1$ in scaled units) using Eq. (4.23).
- From the values of $U_\pm$, the probability of jumping towards the +end of the tube, p_+, is calculated using Eq. (4.55).
- To obtain the direction of the next jump, we compare the probability p_+ with a random number between 0 and 1.
- Once the direction is known, we calculate the mean duration t_+ (or t_-) and the variance Δt_+^2 (or Δt_-^2) of the jumping process as well as the angle Θ of the new tube section.
- The chain is then moved in its tube in the selected ($\pm$) direction and the position of the previously occupied opposite extremity (the segment at the $\mp$end of the tube) is lost. The current time is increased by $t_+ \pm \Delta t_+$ for a forward jump, or is increased by $t_- \pm \Delta t_-$ for a backward jump (the $\pm$ in front of the standard deviations is selected randomly).
- We finally update the energy vector as well as the position vector for the new tube sections.

This cycle is repeated until the steady-state is reached (which may require millions of iterations if g is large). To facilitate the calculations, the distance traveled by a fragment is expressed in units of the pore size parameter a and the times in units of τ_B/N (the Brownian time per primitive segment). After a certain time, we calculate the average electrophoretic velocity of the probes $\langle v \rangle$ and the average x-component of the diffusion coefficient of the system $\langle D_x \rangle$. The

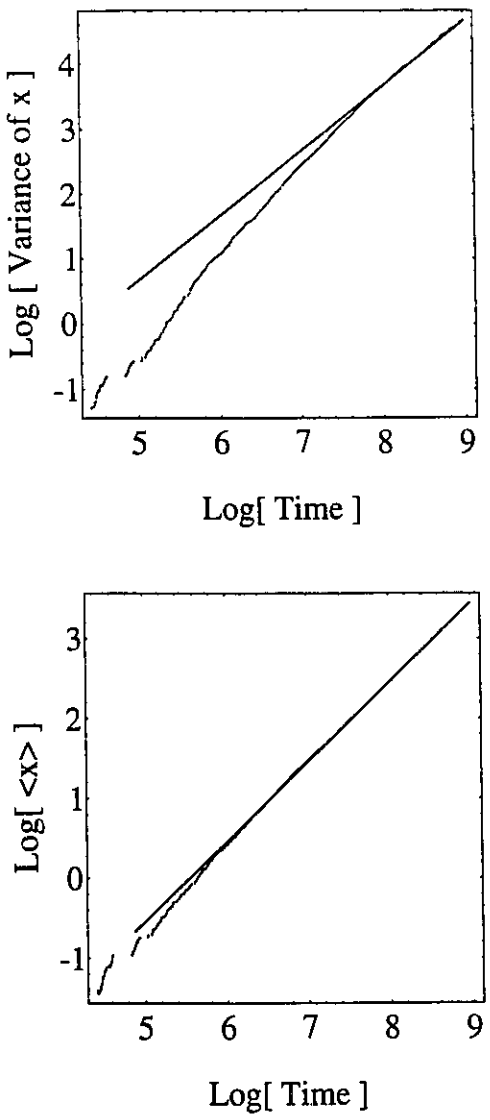

Figure 4.11 The Transient Regime
The first figure shows the variance of x, $\langle \Delta x^2 \rangle$, as a function of time t . The second figure shows the mean distance $\langle x \rangle$ traveled by the polymers as a function of time t. The simulation was done using N=50, ϵ=0.05, ensemb=1000 and g=3.0.

simulation stops when the system has reached a steady-state for both $\langle v \rangle$ and $\langle D_x \rangle$. Figure 4.11 shows a plot of the mean distance $\langle x \rangle$ traveled by the polymers during electrophoresis as well as a plot of the variance $\langle \Delta x^2 \rangle$ as a function of time t. Before reaching the steady-state, we observe a transient regime where neither $\langle x \rangle$ nor $\langle \Delta x^2 \rangle$ increases linearly with time; these transient

regimes are typical of diffusion processes in non-homogeneous systems and were not studied. Note, however, that the duration of these transient regimes increases with the size of the polymer and the value of the energy parameter g. In some cases, it has been impossible to reach the steady-state in a reasonable simulation time and for a meaningful ensemble size.

4.6 Results

4.6.1 Testing the Algorithm

We first verify that our simulations, when used without trapping (g=0), give the same results as the normal biased reptation theory [51-53]. The test results are shown in Figs. 4.12 and

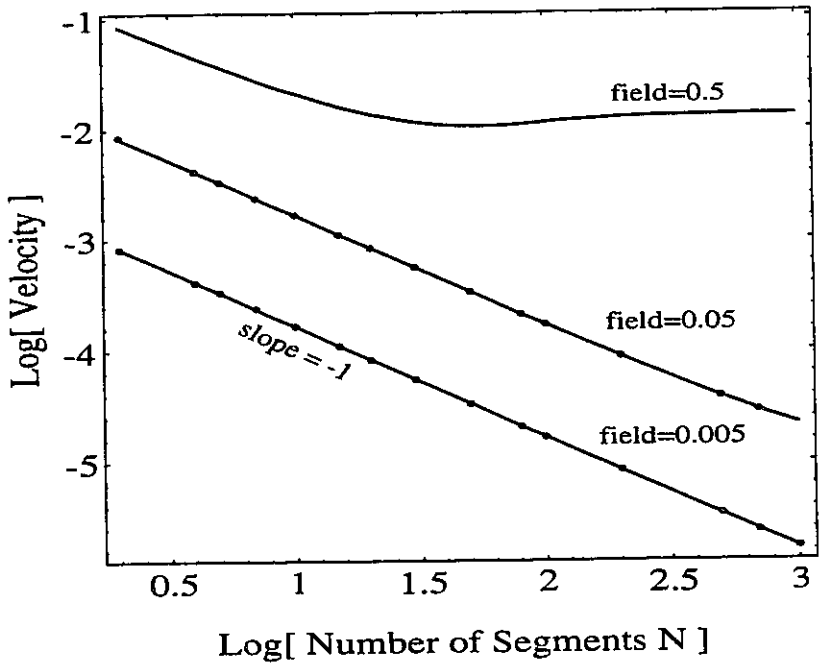

Figure 4.12 Velocity vs. Number of Segments N
Log-log plot of the electrophoretic velocity against the size of the polymer N without trapping (g=0). The solid lines come from the reptation theory [51-53] and the points are obtained from computer simulations. The ϵ=0.5 curve has been drawn for reference.

4.13, where the velocity and the diffusion coefficient are plotted against the number of segments (N) of the macro ions for different electric field intensities ϵ. One can see that the velocity (Fig. 4.12) is strictly proportional to the inverse of N for low fields or small molecules. For higher electric fields or larger polymers, the velocity plateaus to a value $\approx \epsilon^3/9$ [73]. The diffusion coefficient (Fig. 4.13) is composed of three distinct regimes: for low fields/small molecules, the diffusion coefficient is directly proportional to N^{-2}; for very high fields/large polymers, the diffusion coefficient plateaus; between these two regions, the diffusion coefficient is first proportional to $N^{-1/2}$ and then goes through a broad maximum. The agreement between the simulation results (points) and the "exact" analytical results of the theory (solid lines) in Figs. 4.12

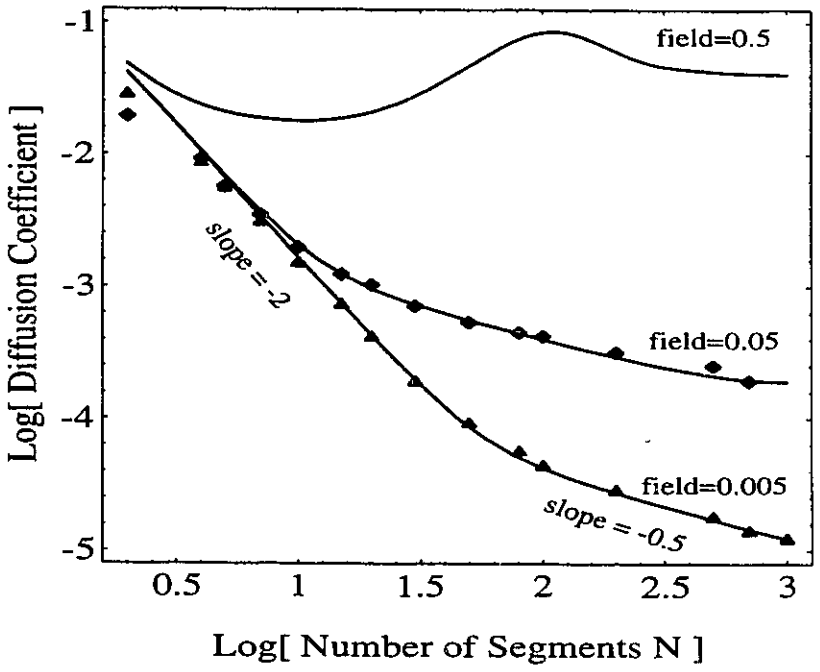

Figure 4.13 Diffusion Coefficient vs. Number of Segments N
Log-log plot of the diffusion coefficient against the length of the polymer N for cases without trapping (g=0). The solid lines come from the reptation theory [73] and the points are obtained from computer simulations. The ϵ=0.5 curve has been drawn for reference.

and 4.13 tells us that the method works correctly. Note that in Fig. 4.13, the small deviations from the curve are a result of the theoretical assumption that the same end of the polymer is always leading the migration; such an assumption is not valid for very small molecules.

4.6.2 The Electrophoretic Velocity in an Irregular Matrix

We now investigate the effects of local free energies on the reptation dynamics of polymers. Figure 4.14 is a log-log plot of the velocity vs. the size of the polymer (N), with the standard deviation of the segmental energies set to g=3.0 (in scaled units), for different field intensities ϵ. We chose this large value of g in order to obtain clear effects. Figure 4.15 gives the

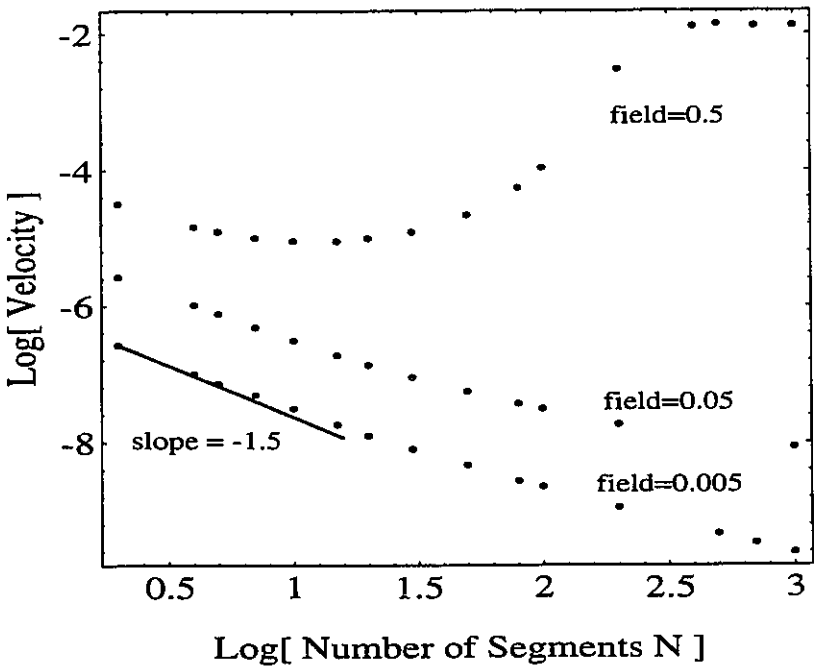

Figure 4.14 Velocity vs. Number of Segments N for g=3.0
Log-log plot of the electrophoretic velocity against the size N of the polymer with trapping effects (g=3). The points are obtained from computer simulations using the new model. A solid line with a slope of -1.5 is also shown.

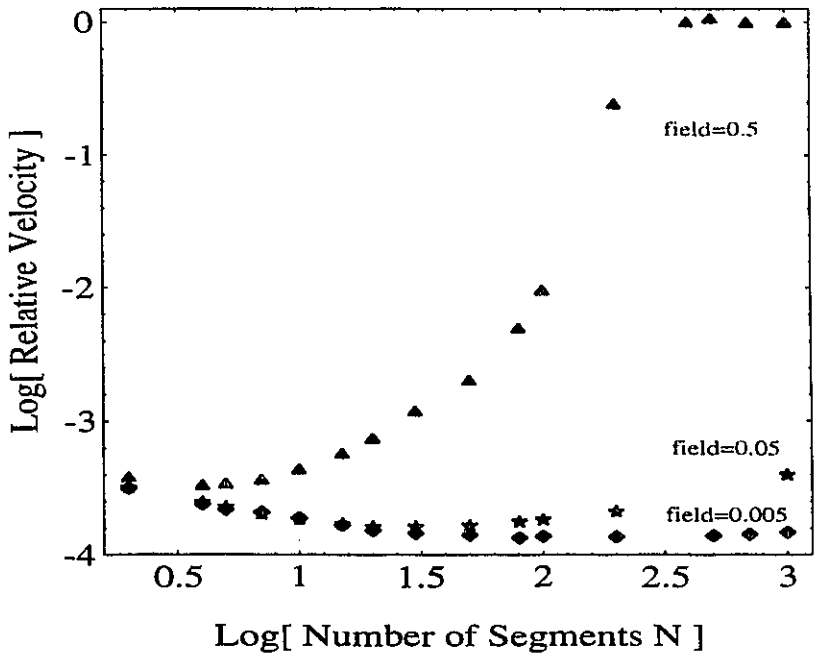

Figure 4.15 Relative Velocity vs. Number of Segments
Log-log plot of the relative velocity ($V_{g=3}/V_{g=0}$) against the size of the polymer N.

relative electrophoretic velocities ($V_{g=3}/V_{g=0}$) of the polymer as a function of N. The main effects of the local free energies are observed to be the following:

- For low field intensities or for small polyelectrolytes, the velocities are many orders of magnitude lower than they would be without trapping, i.e. g=0 (see Fig. 4.15). Indeed, while the minimum time for a jump is zero, there is no maximum when traps are present. Random energies thus tend to slow the dynamics of the polymers.
- The inverse first law predicted by the reptation theory for small DNA fragments is not applicable when g≠0 (see Fig. 4.14). In our simulations, the velocity, for small molecules, approaches a dependence as high as the -1.5 power of the length of the polymer (N < 10). This result agrees very well with the experimental data obtained by Mayer et al. in

polyacrylamide gels [59]. These authors found that the electrophoretic velocity can decrease as fast as $N^{-1.6}$ for similarly small DNA molecules (roughly for $N < 15$).

- For $g=0$, it is well known that the velocity goes through a shallow minimum at $N_{min} \cong 14/\epsilon^2$ [73] before saturating at a slightly higher value. This minimum seems to shift to a smaller size N_{min} when the effect of trapping is present. This can be seen by comparing Figs. 4.12 and 4.14 for $\epsilon=0.05$ and $\epsilon=0.5$.
- For very large molecular sizes/electric field intensities, the velocity of the polyelectrolyte (with trapping) reaches the same plateau whether or not $g=0$. This could lead to very strong "band inversion", where larger polymers move faster than smaller ones (see Fig. 4.14 for $\epsilon=0.5$). Such inversions have been observed by Jean Rousseau (presently the PDF in Guy Drouin's laboratory, Department of Biology, University of Ottawa), who found $N_{min} \simeq 1200$ bases$\simeq 17$ reptation segments in a polyacrylamide gel.
- As mentioned before, if the field intensity is too high, the local interactions have no effects on the velocity of the polymer. In other words, if $\epsilon \to \infty$, the electrophoretic velocity of the polyelectrolytes is the same with or without trapping since the electric forces can easily overwhelm the energy trap.

Unlike the results obtained by ZL [19], the local free energies used in this model have important effects on small molecules (ZL found important effects only for intermediate sizes). The difference between the two models comes from the definition of the energy model; in the local free energy model, the difference ΔE between the free energy of two conformations scales as N^0 whereas in ZL's energy barrier model, ΔE is proportional to $N^{1/2}$. Since the electric forces F_ϵ are strictly proportional to the length of the molecules $N^{1.0}$, both models must converge towards the $g=0$ limit for high field intensities or large molecular sizes. We do indeed observe this behavior for both models (see Figs. 4.6 and 4.15). Thus, the local free energy interactions become more significant for small DNA fragments ($\Delta E \propto N^0$, $F_\epsilon \propto N^{1.0}$) whereas the effect of ZL's energy barriers are more significant for intermediate sizes ($\Delta E \propto N^{1/2}$, $F_\epsilon \propto N^{1.0}$).

4.6.3 The Diffusion Coefficient in an Irregular Matrix

Figure 4.16 shows a log-log plot of the diffusion coefficient against the size N of the

polymer for different field intensities ϵ with a standard deviation of the segmental energies set to g=3.0 (in scaled units). Figure 4.17 shows the ratio $D_{g=3}/D_{g=0}$ as a function of the molecular size N. Note that we do not have data points for sizes larger than N=100 for ϵ=0.5 since the steady-state could not be reached (in spite of many days of CPU time). The main effects of the local free energies are observed to be the following:

- For low field intensities/small polyelectrolytes, the diffusion coefficients are many orders of magnitude lower than without trapping, i.e. g=0 (see Fig. 4.17). Such a reduction of the diffusion coefficient was found by Muthukumar and Baumgärtner [71, 72] in their zero-field model of entropic barriers.

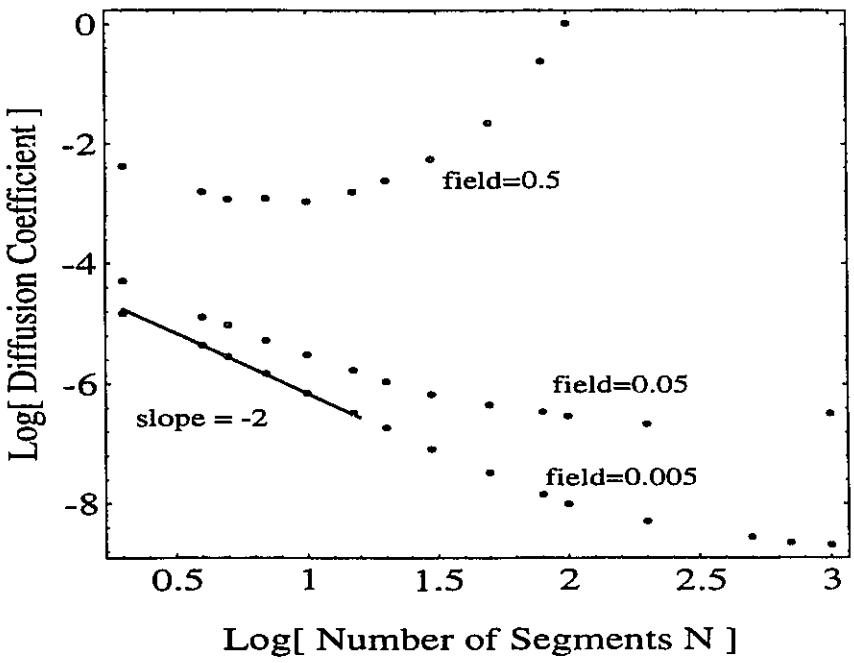

Figure 4.16 Diffusion Coefficient vs. Number of Segments for g = 3.0
Log-log plot of the diffusion coefficient against the size N of the polymer with trapping effects (g=3). The points are obtained from computer simulations using the new model. A solid line with a slope of -2 is also shown.

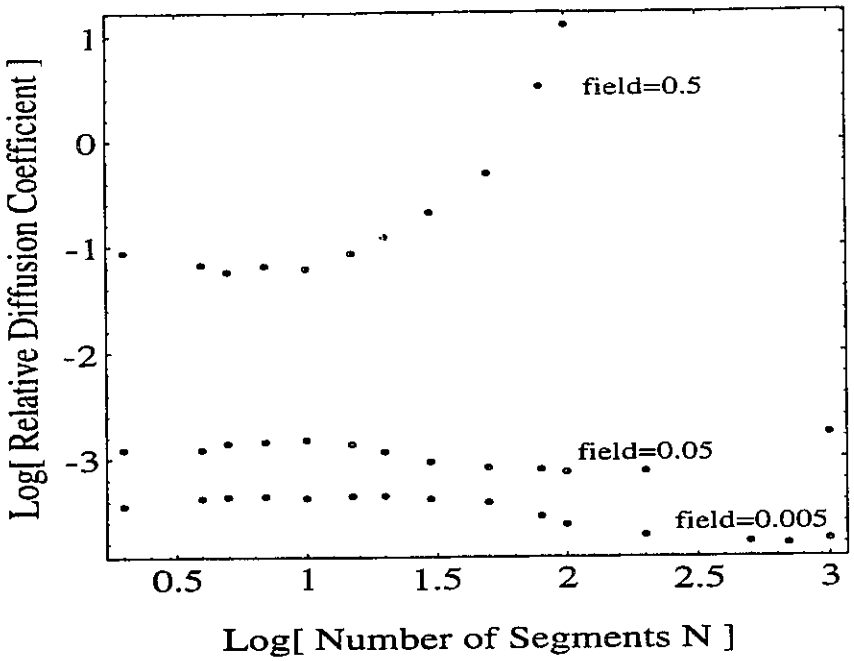

Figure 4.17 Relative Diffusion Coefficient vs. Number of Segments
Log-log plot of the relative diffusion coefficient ($D_{g=3}/D_{g=0}$) against the size of the polymer N.

- Like in the standard (g=0) reptation model [51-53], the diffusion coefficient is first proportional to N^{-2} for low fields/small molecules (see Fig. 4.16), and then becomes proportional to $N^{-1/2}$.
- Unlike ZL [19], we do not find a dramatic change of power laws in the zero-field limit ($\epsilon \to 0$). In fact, the power laws remain almost the same (see Fig. 4.17 for $\epsilon=0.05$ and $\epsilon=0.005$).
- Typical diffusion coefficient vs. molecular size curves go through a shallow minimum as well as a maximum before saturating at a higher value. The minimum seems to shift towards smaller molecular size values when the effect of trapping is present while the maximum seems to shift towards larger sizes. This can be seen by comparing Figs. 4.13 and 4.16 for $\epsilon=0.05$ and 0.5.

- For very large molecular sizes/high electric fields, the diffusion coefficient of the polymer increases by many orders of magnitude (see Figs. 4.16 and 4.17).
- Also, the diffusion coefficient seems to become more field-dependent when trapping is present (compare Figs. 4.13 and 4.16). This is a very important feature of this new model.

The most surprising finding here is the fact that the relative diffusion coefficient exceeds 0.0 for large field intensities (see Fig. 4.17 for $\epsilon=0.5$). This effect is related to the high velocity of large molecules (Fig. 4.14 for $\epsilon=0.5$). In strong electric fields, the total force ($\propto \epsilon h_x/a$) acting on the molecule is usually very large compare to the random energy term (which is of order g). Therefore, long molecules encounter very few deep traps and their velocities are barely affected. However, the end-to-end distance fluctuates with time and one occasionally has $\epsilon h_x/a << g$; in this case, the escape time is very large. Although these deep traps are rare, they strongly affect the diffusion for the following reason; when a molecule is trapped, the other free molecules of the same size migrate away at a very high velocity. This secondary diffusion process, typical of systems with high velocities between deep traps, leads to a diffusion coefficient larger than the one that characterizes the motion between the deep traps. This effect has been observed in other systems (Hong Guo, M. Sc. Thesis, University of Ottawa, 1994; Claude Desruisseaux, M. Sc. Thesis, University of Ottawa, 1994).

4.7 Conclusion

In this chapter, we presented a new theoretical approach to gel electrophoresis of polyelectrolytes in irregular matrices. The first model, proposed by Zimm and Lumpkin [19], was based on a modified reptation theory [51-53] with random energy fluctuations. These fluctuations correspond to an effective energy barrier model. However, the ZL model did not take into account the well-known memory effects of the reptation model [49]; this could lead to severe artifacts. Zimm and Lumpkin found that even weak interactions between the chain and the gel can complicate the simple reptation picture and can have dramatic effects on both the diffusion coefficient and the electrophoretic velocity. In the case of the electrophoretic velocity, the effect of trapping is more significant for intermediate sizes (see Figs. 4.5 and 4.6). This is due to the very different size dependences of the total interaction free energy ($\Delta G \propto N^{1/2}$) and the total electric

force ($F_\epsilon \propto N^{1.9}$) in Eq. (4.19). The effects of irregular matrices on the diffusion coefficient (for $\epsilon \neg 0$) seem to transform the dependence on N from a power law to an exponential law (see Fig. 4.7) and to reduce the value of the diffusion coefficient. Such a reduction was also found by Muthukumar and Baumgartner [71, 72] in their entropic barrier model.

Our model of gel electrophoresis in irregular matrices is also based on a modified reptation model [51-53] with random energy fluctuations. The main differences between the two models (the ZL model and ours) come from the definition of the energy model which is related, for technical reasons, to the distance migrated by the polymer in the "jumping process". Since we have chosen $\delta x \leq a$ as the step size for the jumps (as opposed to $\delta x = h_x$ in the ZL model), the memory effects present in the reptation model are automatically taken into account. For this reason, we believe that our approach is more reliable.

For small molecules and low field intensities, we found that trapping reduces the electrophoretic velocity (Fig. 4.15). When the electric field (or the size of the polymer) is increased, the effect of the random energy fluctuations decreases and eventually becomes negligible. We also found a $N^{-1.5}$ dependence which agrees well with the results obtained by Mayer et al. [59] for small polymers and low electric fields (see Fig. 4.14). Unlike the ZL model, we do not find a dramatic change in the power laws which govern the diffusion coefficient in the zero-field limit (see Fig. 4.16). However, we do observe a significant decrease in the diffusion coefficient. We also observe a dramatic increase in the diffusion coefficient for high field intensities (Figs. 4.16 and 4.17). This is due to the fact that when a polymer molecule becomes trapped, all the other molecules of the same size move away from it at very high velocities. We predict that the diffusion coefficient as well as the electrophoretic velocity (for $g \neq 0$) will converge towards the values predicted by the reptation theory ($g = 0$) for very large field intensities or very large polymer sizes. We also predict a loss in the quality of the separation process. Figure 4.18 shows the ratio (Relative Velocity/Relative Diffusion Coefficient) plotted against the number of segments. The ratio Velocity/Diffusion Coefficient is a measure of the quality of the separation process. Since all the values shown in Fig. 4.18 are lower or equal to 0.0, it is evident that local free energies always lead to a loss of the quality of separation, especially in the presence of high field intensities.

The next logical step will be to study the energy barrier model instead of the present local

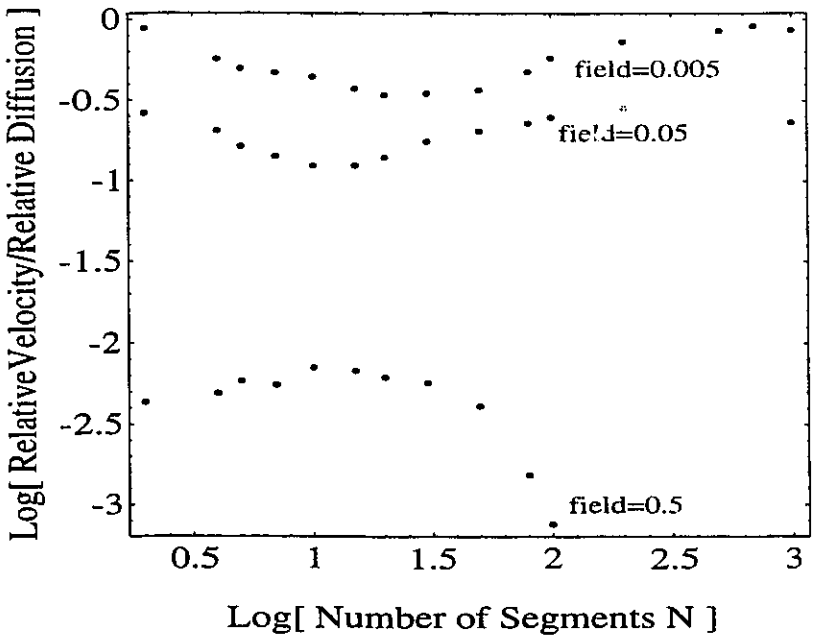

Figure 4.18 Ratio (Relative V / Relative D) vs. N
Log-log plot of the ratio of the relative electrophoretic velocity over the relative diffusion coefficient against the size of the polymer N.

energy model. The results are expected to be quite different since the energy required to perform each "jump" will increase with the size of the molecule ($N^{1.0}$). This model will be closer to ZL's model; however, since our computational approach is quite different, we expect qualitatively different results. At this time, it is too early to compare the theoretical results with experimental data since the models have yet to be understood completely and the experimental data remain quite scarce.

Chapitre 5

Conclusion

Cette thèse comprend une étude théorique de trois problèmes reliés à l'électrophorèse des polyélectrolytes: l'électrophorèse en capillaire d'un complexe ADN-polymère (chapitre 2), l'électrophorèse de la molécule d'ADN en solution polymérique ultra-diluée (chapitre 3), et enfin l'électrophorèse de polyélectrolytes dans un matrice irrégulière (chapitre 4).

Au chapitre 2, nous avons présenté une investigation théorique de ELFSE [9] ("End-Label Free Solution Electrophoresis") où l'étiquette (l'objet attaché à la molécule d'ADN) est un polymère neutre et flexible. Cette étude nous a permis de démontrer qu'un polymère se comporte très différemment d'un objet globulaire (e.g., une protéine) lorsqu'il est employé comme générateur de friction dans ELFSE. En fait, il nous permet d'augmenter le coefficient de friction de la molécule hybride sans changer l'étiquette puisque la déformation du polymère est directement reliée à la vitesse du complexe. Il existe trois principaux régimes de déformation: 1) globulaire, 2) formation de trompette et 3) étirement complet. Dans le premier régime (globulaire), les forces exercées sur le polymère ne sont pas assez grandes pour le déformer. Les résultats obtenus par le groupe de Mayer et al. [9] sont valides pour ce régime. Dans le régime intermédiaire (le plus important), la formation de trompettes, la vitesse électrophorétique ne dépend plus que faiblement du champ électrique et de la masse moléculaire de l'ADN ($M_D^{1/3}$ et $E^{1/3}$). Cette faible dépendance est principalement due au fait que le surplus de force électrique produit par des molécules plus grosses ou des champs électriques plus élevés est utilisé dans la déformation du polymère plutôt que dans l'augmention de la vitesse nette de la molécule hybride. Les Figs. 2.3 et 2.4 démontrent clairement que l'intervalle de masses d'ADN que l'on peut séparer est beaucoup plus large dans le régime intermédiaire. Dans le dernier régime, les forces exercées sur le polymère sont assez élevées pour que celui-ci s'étire complètement. Ce régime augmente également l'intervalle de masses d'ADN que l'on peut séparer. Il est à noter ici que le groupe de Guy Drouin (Département de Biologie à l'Université d'Ottawa) sera en mesure de vérifier nos prédictions dans les prochains mois.

Au chapitre 3, nous avons proposé un modèle théorique de l'électrophorèse de l'ADN dans une solution polymérique ultra-diluée basé sur les résultats expérimentaux obtenus par Barron et al. [8]. Puisque ces résultats ne peut être expliqués par un simple prolongement du modèle d'Ogston [50] ou même du modèle de la reptation [51-53], nous avons élaboré un nouveau modèle en se basant sur l'hydrodynamique et les collisions moléculaires. Tout comme Barron et al. [8], nous suggérons que les polymères s'attachent temporairement à la molécule d'ADN lorsque ceux-ci entrent en collision. Le processus d'enchevêtrement et de détachement d'un polymère autour de ADN (et vice-versa) est au coeur du processus de séparation. Présentement, les limites de cette nouvelle technique de séparation sont pratiquement inconnues. Toutefois, il est clair que les vitesses électrophorétiques nettes permises par cette technique sont largement supérieures à celles obtenues en utilisant l'électrophorèse dans une plaque de gel [6]. Si une résolution semblable pouvait être réalisée en solution ultra-diluée, nous aurions permis une amélioration majeure des techniques de séparation électrophorétiques pour le projet du génome humain. Nous travaillons présentement à la généralisation du modèle afin d'inclure les effets spécifiques aux polymères beaucoup plus longs, aux conformations en trompettes, ainsi que le régime hyper-dilué où l'on a en moyenne moins d'un polymère attaché à l'ADN durant la migration.

Au chapitre 4, nous avons comparé deux modèles de l'électrophorèse de polyélectrolytes dans un matrice irrégulière. Le premier, proposé par Zimm et Lumpkin [19], est basé sur la théorie de la reptation [51-53] avec des fluctuations énergétiques aléatoires. Ces auteurs ont remarqué que même une faible interaction entre le polyélectrolyte et le gel peut compliquer la dynamique et avoir des effets majeurs sur la vitesse ainsi que sur le coefficient de diffusion. Les pincipaux effets observés par ZL sont: 1) une réduction des vitesses électrophorétiques, 2) les vitesses des tailles moléculaires intermédiaires ont une dépendance envers N, la taille moléculaire, plus élevée (environ N^{-3}) que celle prédite (N^{-1}) par le modèle standard de la reptation [51-53] et 3) le coefficient de diffusion semble passer d'une loi de puissance (N^{-2}) à une loi exponentielle. Notre nouveau modèle est également basé sur un modèle de reptation [51-53] auquel on a ajouté des fluctuations énergétiques aléatoires. Les principales différences entre notre modèle et celui de ZL [19] sont: 1) la définition du modèle d'énergie utilisée et 2) la longueur des sauts discrets dans le processus du mouvement de la chaîne. Puisque la longueur des sauts est petite ($\delta x \leq a$) dans

notre modèle, ce dernier tient compte de l'effet de mémoire du modèle de la reptation. Cet effet disparaît si la distance entre chaque saut devient trop grande (Zimm et Lumpkin ont utilisé $\delta x \approx h_x$). Pour cette raison, nous considérons notre approche plus fiable. Les principaux effets que nous avons observés sont: 1) une réduction des vitesses électrophorétiques, 2) les vitesses des petites tailles moléculaires ont une dépendance envers la taille moléculaire plus élevée ($N^{-1.5}$) que celle prédite (N^{-1}) par le modèle standard de la reptation [51-53], 3) la loi de puissance du coefficient de diffusion ne semble pas changer de façon signifivative pour les petites masses moléculaires ou les faibles champs électriques, et 4) une augmentation prononcée du coefficient de diffusion pour des champs électriques élevés. Nous essayons présentement d'expliquer les différents résultats expérimentaux obtenus par le groupe de Guy Drouin de l'Université d'Ottawa. Nous espérons également changer la nature du modèle d'énergie utilisé (énergie locales vs. barrières d'énergie) dans un avenir rapproché afin de mieux comprendre l'électrophorèse des polyélectrolytes dans des matrices irrégulières.

Appendix A

For an irregular matrix (see Fig. 4.9), the expression for the mean exit time is obtained using Eqs. (4.44), (4.45), (4.46), (4.56) and (4.57):

$$
\begin{aligned}
\langle t_{\pm} \rangle = {} & (x_{\pm}*(-2*D_c*U_{\mp}^2*x_{\pm}^2+2*D_c*\exp(U_{\pm}/D_c)*U_{\mp}^2*x_{\pm}^2+2*D_c*\exp(U_{-}+/D_c)*U_{\mp}^2*x_{\pm}^2- \\
& 2*D_c*\exp((U_{\pm}+U_{\mp})/D_c)*U_{\mp}^2*x_{\pm}^2-U_{\pm}*U_{\mp}^2*x_{\pm}^2-\exp(U_{\pm}/D_c)*U_{\pm}*U_{\mp}^2*x_{\pm}^2+ \\
& \exp(U_{\mp}/D_c)*U_{\pm}*U_{\mp}^2*x_{\pm}^2+\exp((U_{\pm}+U_{\mp})/D_c)*U_{\pm}*U_{\mp}^2*x_{\pm}^2+D_c*U_{\pm}*U_{\mp}*x_{\pm}*x_{\mp}- \\
& D_c*\exp(U_{\pm}/D_c)*U_{\pm}*U_{\mp}*x_{\pm}*x_{\mp}-2*D_c*\exp(U_{\mp}/D_c)*U_{\pm}*U_{\mp}*x_{\pm}*x_{\mp}+ \\
& D_c*\exp((2*U_{\mp})/D_c)*U_{\pm}*U_{\mp}*x_{\pm}*x_{\mp}+2*D_c*\exp((U_{\pm}+U_{\mp})/D_c)*U_{\pm}*U_{\mp}*x_{\pm}*x_{\mp}- \\
& D_c*\exp((U_{\pm}+2*U_{\mp})/D_c)*U_{\pm}*U_{\mp}*x_{\pm}*x_{\mp}+U_{\pm}^2*U_{\mp}*x_{\pm}*x_{\mp}- \\
& 2*\exp(U_{\mp}/D_c)*U_{\pm}^2*U_{\mp}*x_{\pm}*x_{\mp}+\exp((2*U_{\mp})/D_c)*U_{\pm}^2*U_{\mp}*x_{\pm}*x_{\mp}+D_c*U_{\pm}^2*x_{\mp}^2- \\
& D_c*\exp(U_{\pm}/D_c)*U_{\pm}^2*x_{\mp}^2-D_c*\exp((2*U_{\mp})/D_c)*U_{\pm}^2*x_{\mp}^2+ \\
& D_c*\exp((U_{\pm}+2*U_{\mp})/D_c)*U_{\pm}^2*x_{\mp}^2+2*\exp(U_{\mp}/D_c)*U_{\pm}^2*U_{\mp}*x_{\mp}^2- \\
& 2*\exp((U_{\pm}+U_{\mp})/D_c)*U_{\pm}^2*U_{\mp}*x_{\mp}^2))/ \\
& ((1-\exp(U_{\mp}/D_c))*U_{\pm}^2*U_{\mp}*(U_{\mp}*x_{\pm}-\exp(U_{\pm}/D_c)*U_{\mp}*x_{\pm}-U_{\pm}*x_{\mp}+\exp(U_{\mp}/D_c)*U_{\pm}*x_{\mp}))
\end{aligned}
$$

This expression has been obtained using Mathematica. Note that we have assumed that the particle is initially at the origin ($x=0$). In our simulation program, we use $x_{\pm}=\pm 1$ and $D_c=1$, while $U_{\pm}$ is given by Eq. (4.23).

The second moment of the exit time using Eqs. (4.49), (4.50), (4.46), (4.56) and (4.57) is:

$$\begin{aligned}\left\langle \Delta t_{\pm}^{2} \right\rangle = {} & (x_{\pm}(4D_c^2U_{\mp}^5x_{\pm}^5 - 4aD_c^2U_{\mp}^5x_{\pm}^5 - 8bD_c^2U_{\mp}^5x_{\pm}^5 + 8abD_c^2U_{\mp}^5x_{\pm}^5 + 4b^2D_c^2U_{\mp}^5x_{\pm}^5 - \\ & 4ab^2D_c^2U_{\mp}^5x_{\pm}^5 - 2D_cU_{\pm}U_{\mp}^5x_{\pm}^5 + 2aD_cU_{\pm}U_{\mp}^5x_{\pm}^5 + 2b^2D_cU_{\pm}U_{\mp}^5x_{\pm}^5 - 2ab^2D_cU_{\pm}U_{\mp}^5x_{\pm}^5 - \\ & U_{\pm}^2U_{\mp}^5x_{\pm}^5 + aU_{\pm}^2U_{\mp}^5x_{\pm}^5 - 6bU_{\pm}^2U_{\mp}^5x_{\pm}^5 + 6abU_{\pm}^2U_{\mp}^5x_{\pm}^5 - b^2U_{\pm}^2U_{\mp}^5x_{\pm}^5 + \\ & ab^2U_{\pm}^2U_{\mp}^5x_{\pm}^5 - 10D_c^2U_{\pm}U_{\mp}^4x_{\pm}^4x_{\mp} + 20aD_c^2U_{\pm}U_{\mp}^4x_{\pm}^4x_{\mp} - 10a^2D_c^2U_{\pm}U_{\mp}^4x_{\pm}^4x_{\mp} + \\ & 8bD_c^2U_{\pm}U_{\mp}^4x_{\pm}^4x_{\mp} - 16abD_c^2U_{\pm}U_{\mp}^4x_{\pm}^4x_{\mp} + 8a^2bD_c^2U_{\pm}U_{\mp}^4x_{\pm}^4x_{\mp} + 2b^2D_c^2U_{\pm}U_{\mp}^4x_{\pm}^4x_{\mp} - \\ & 4ab^2D_c^2U_{\pm}U_{\mp}^4x_{\pm}^4x_{\mp} + 2a^2b^2D_c^2U_{\pm}U_{\mp}^4x_{\pm}^4x_{\mp} + 2D_cU_{\pm}^2U_{\mp}^4x_{\pm}^4x_{\mp} - 4aD_cU_{\pm}^2U_{\mp}^4x_{\pm}^4x_{\mp} + \\ & 2a^2D_cU_{\pm}^2U_{\mp}^4x_{\pm}^4x_{\mp} - 12bD_cU_{\pm}^2U_{\mp}^4x_{\pm}^4x_{\mp} + 24abD_cU_{\pm}^2U_{\mp}^4x_{\pm}^4x_{\mp} - 12a^2bD_cU_{\pm}^2U_{\mp}^4x_{\pm}^4x_{\mp} - \\ & 2b^2D_cU_{\pm}^2U_{\mp}^4x_{\pm}^4x_{\mp} + 4ab^2D_cU_{\pm}^2U_{\mp}^4x_{\pm}^4x_{\mp} - 2a^2b^2D_cU_{\pm}^2U_{\mp}^4x_{\pm}^4x_{\mp} + 2U_{\pm}^3U_{\mp}^4x_{\pm}^4x_{\mp} - \\ & 4aU_{\pm}^3U_{\mp}^4x_{\pm}^4x_{\mp} + 2a^2U_{\pm}^3U_{\mp}^4x_{\pm}^4x_{\mp} + 6bU_{\pm}^3U_{\mp}^4x_{\pm}^4x_{\mp} - 12abU_{\pm}^3U_{\mp}^4x_{\pm}^4x_{\mp} + \\ & 6a^2bU_{\pm}^3U_{\mp}^4x_{\pm}^4x_{\mp} + 8D_c^2U_{\pm}^2U_{\mp}^3x_{\pm}^3x_{\mp}^2 - 12aD_c^2U_{\pm}^2U_{\mp}^3x_{\pm}^3x_{\mp}^2 + 8a^2D_c^2U_{\pm}^2U_{\mp}^3x_{\pm}^3x_{\mp}^2 - \\ & 4a^3D_c^2U_{\pm}^2U_{\mp}^3x_{\pm}^3x_{\mp}^2 - 10bD_c^2U_{\pm}^2U_{\mp}^3x_{\pm}^3x_{\mp}^2 + 6abD_c^2U_{\pm}^2U_{\mp}^3x_{\pm}^3x_{\mp}^2 + 2a^2bD_c^2U_{\pm}^2U_{\mp}^3x_{\pm}^3x_{\mp}^2 + \\ & 2a^3bD_c^2U_{\pm}^2U_{\mp}^3x_{\pm}^3x_{\mp}^2 + 2b^2D_c^2U_{\pm}^2U_{\mp}^3x_{\pm}^3x_{\mp}^2 + 6ab^2D_c^2U_{\pm}^2U_{\mp}^3x_{\pm}^3x_{\mp}^2 - \\ & 10a^2b^2D_c^2U_{\pm}^2U_{\mp}^3x_{\pm}^3x_{\mp}^2 + 2a^3b^2D_c^2U_{\pm}^2U_{\mp}^3x_{\pm}^3x_{\mp}^2 + 2D_cU_{\pm}^3U_{\mp}^3x_{\pm}^3x_{\mp}^2 - \\ & 2a^2D_cU_{\pm}^3U_{\mp}^3x_{\pm}^3x_{\mp}^2 + 6bD_cU_{\pm}^3U_{\mp}^3x_{\pm}^3x_{\mp}^2 - 18abD_cU_{\pm}^3U_{\mp}^3x_{\pm}^3x_{\mp}^2 + 18a^2bD_cU_{\pm}^3U_{\mp}^3x_{\pm}^3x_{\mp}^2 - \\ & 6a^3bD_cU_{\pm}^3U_{\mp}^3x_{\pm}^3x_{\mp}^2 - 2b^2D_cU_{\pm}^3U_{\mp}^3x_{\pm}^3x_{\mp}^2 + 2a^2b^2D_cU_{\pm}^3U_{\mp}^3x_{\pm}^3x_{\mp}^2 - U_{\pm}^4U_{\mp}^3x_{\pm}^3x_{\mp}^2 + \\ & 3aU_{\pm}^4U_{\mp}^3x_{\pm}^3x_{\mp}^2 - 3a^2U_{\pm}^4U_{\mp}^3x_{\pm}^3x_{\mp}^2 + a^3U_{\pm}^4U_{\mp}^3x_{\pm}^3x_{\mp}^2 + 8aD_cU_{\pm}^2U_{\mp}^4x_{\pm}^3x_{\mp}^2 - \\ & 16abD_cU_{\pm}^2U_{\mp}^4x_{\pm}^3x_{\mp}^2 + 8ab^2D_cU_{\pm}^2U_{\mp}^4x_{\pm}^3x_{\mp}^2 + 4aU_{\pm}^3U_{\mp}^4x_{\pm}^3x_{\mp}^2 - 4ab^2U_{\pm}^3U_{\mp}^4x_{\pm}^3x_{\mp}^2 + \\ & 4bD_c^2U_{\pm}^3U_{\mp}^2x_{\pm}^2x_{\mp}^3 - 4abD_c^2U_{\pm}^3U_{\mp}^2x_{\pm}^2x_{\mp}^3 - 4a^2bD_c^2U_{\pm}^3U_{\mp}^2x_{\pm}^2x_{\mp}^3 + 4a^3bD_c^2U_{\pm}^3U_{\mp}^2x_{\pm}^2x_{\mp}^3 - \\ & 4b^2D_c^2U_{\pm}^3U_{\mp}^2x_{\pm}^2x_{\mp}^3 + 4ab^2D_c^2U_{\pm}^3U_{\mp}^2x_{\pm}^2x_{\mp}^3 + 4a^2b^2D_c^2U_{\pm}^3U_{\mp}^2x_{\pm}^2x_{\mp}^3 - \\ & 4a^3b^2D_c^2U_{\pm}^3U_{\mp}^2x_{\pm}^2x_{\mp}^3 - 2D_cU_{\pm}^4U_{\mp}^2x_{\pm}^2x_{\mp}^3 + 2aD_cU_{\pm}^4U_{\mp}^2x_{\pm}^2x_{\mp}^3 + 2a^2D_cU_{\pm}^4U_{\mp}^2x_{\pm}^2x_{\mp}^3 - \\ & 2a^3D_cU_{\pm}^4U_{\mp}^2x_{\pm}^2x_{\mp}^3 + 6bD_cU_{\pm}^4U_{\mp}^2x_{\pm}^2x_{\mp}^3 - 6abD_cU_{\pm}^4U_{\mp}^2x_{\pm}^2x_{\mp}^3 - 6a^2bD_cU_{\pm}^4U_{\mp}^2x_{\pm}^2x_{\mp}^3 + \\ & 6a^3bD_cU_{\pm}^4U_{\mp}^2x_{\pm}^2x_{\mp}^3 + 8abD_cU_{\pm}^3U_{\mp}^3x_{\pm}^2x_{\mp}^3 - 8a^2bD_cU_{\pm}^3U_{\mp}^3x_{\pm}^2x_{\mp}^3 - 8ab^2D_cU_{\pm}^3U_{\mp}^3x_{\pm}^2x_{\mp}^3 + \\ & 8a^2b^2D_cU_{\pm}^3U_{\mp}^3x_{\pm}^2x_{\mp}^3 - 4aU_{\pm}^4U_{\mp}^3x_{\pm}^2x_{\mp}^3 + 4a^2U_{\pm}^4U_{\mp}^3x_{\pm}^2x_{\mp}^3 + 12abU_{\pm}^4U_{\mp}^3x_{\pm}^2x_{\mp}^3 - \\ & 12a^2bU_{\pm}^4U_{\mp}^3x_{\pm}^2x_{\mp}^3 - 4D_c^2U_{\pm}^4U_{\mp}x_{\pm}x_{\mp}^4 - 2aD_c^2U_{\pm}^4U_{\mp}x_{\pm}x_{\mp}^4 + 4a^2D_c^2U_{\pm}^4U_{\mp}x_{\pm}x_{\mp}^4 + \\ & 2a^3D_c^2U_{\pm}^4U_{\mp}x_{\pm}x_{\mp}^4 + 8bD_c^2U_{\pm}^4U_{\mp}x_{\pm}x_{\mp}^4 + 4abD_c^2U_{\pm}^4U_{\mp}x_{\pm}x_{\mp}^4 - 8a^2bD_c^2U_{\pm}^4U_{\mp}x_{\pm}x_{\mp}^4 - \\ & 4a^3bD_c^2U_{\pm}^4U_{\mp}x_{\pm}x_{\mp}^4 - 4b^2D_c^2U_{\pm}^4U_{\mp}x_{\pm}x_{\mp}^4 - 2ab^2D_c^2U_{\pm}^4U_{\mp}x_{\pm}x_{\mp}^4 + 4a^2b^2D_c^2U_{\pm}^4U_{\mp}x_{\pm}x_{\mp}^4 +\end{aligned}$$

$$2a^3b^2D_c^2U_\pm^4U_\mp x_\pm x_\mp^4 - 4aD_cU_\pm^4U_\mp^2x_\pm x_\mp^4 - 8a^2D_cU_\pm^4U_\mp^2x_\pm x_\mp^4 + 8abD_cU_\pm^4U_\mp^2x_\pm x_\mp^4 + 16a^2bD_cU_\pm^4U_\mp^2x_\pm x_\mp^4 - 4ab^2D_cU_\pm^4U_\mp^2x_\pm x_\mp^4 - 8a^2b^2D_cU_\pm^4U_\mp^2x_\pm x_\mp^4 + 4aU_\pm^4U_\mp^3x_\pm x_\mp^4 - 8abU_\pm^4U_\mp^3x_\pm x_\mp^4 + 4ab^2U_\pm^4U_\mp^3x_\pm x_\mp^4 + 2D_c^2U_\pm^5x_\mp^5 - 2aD_c^2U_\pm^5x_\mp^5 - 2a^2D_c^2U_\pm^5x_\mp^5 + 2a^3D_c^2U_\pm^5x_\mp^5 - 2bD_c^2U_\pm^5x_\mp^5 + 2abD_c^2U_\pm^5x_\mp^5 + 2a^2bD_c^2U_\pm^5x_\mp^5 - 2a^3bD_c^2U_\pm^5x_\mp^5 - 4aD_cU_\pm^5U_\mp x_\mp^5 + 4a^2D_cU_\pm^5U_\mp x_\mp^5 + 4abD_cU_\pm^5U_\mp x_\mp^5 - 4a^2bD_cU_\pm^5U_\mp x_\mp^5 - 4aU_\pm^5U_\mp^2x_\mp^5 - 4a^2U_\pm^5U_\mp^2x_\mp^5 + 4abU_\pm^5U_\mp^2x_\mp^5 + 4a^2bU_\pm^5U_\mp^2x_\mp^5)) / ((-1 + a)U_\pm^4U_\mp^3(U_\mp x_\pm - bU_\mp x_\pm - U_\pm x_\mp + aU_\pm x_\mp)^2)$$

where the parameter 'a' and 'b' are defined as:

$$a = e^{U_\mp/D_c} \qquad b = e^{U_\pm/D_c}$$

REFERENCES

[1] J.D. Watson and F.H.C. Cick, Nature **171**, 737 (1953).

[2] M.F. Wilkins and J.J. Randall, Nature 171, 738 (1953).

[3] J.D. Watson, *The double helix*, New American Library, New York (1968).

[4] M.V. Olson, Proc. Nalt. Acad. Sci. USA **90**, 4338 (1993).

[5] U.S. Departement of Health and Human Services & U.S. Depatement of Enegy, *Understanding Our Genetic Inheritance, The U.S. Human Genome Project: The Fist Five Years* (1990).

[6] J. L. Viovy and J. Lesec, Advances in Polymer science **114**, 1 (1994).

[7] D.C. Schwatrz and C.R. Cantor, Cell **37**, 67 (1984).

[8] A. E. Barron, H.W. Blanch and D. S. Soane, Electrophoresis **15**, 597 (1994).

[9] P. Mayer, G. W. Slater and G. Drouin, Anal. Chem. **66**, 1777 (1994).

[10] A. S. Cohen, D. L. Smisek and P. Keohavong, Trends Anal. Chem. **12**, 195 (1993).

[11] B.T. Chait, R. Wang, R.C. Beavis and S.B.H. Kent, Science **262**, 89 (1993).

[12] M. Barinaga, Science **253**, 1489 (1991).

[13] B. M. Olivera, P. Baine and N. Davidson, Biopolymers **2**, 245 (1964).

[14] L.S. Lerman and H.L. Frisch, Biopolymers **21**, 995 (1982).

[15] T. Maniatis, E.F. Fritsch and J. Sambrook, Molecular Cloning, *A Laboratory Manual*, Cold Spring Harbor, New York:Cold Spring Harbor Laboratory Press (1982).

[16] W.L. Fangman, Nucl. Acids Res. **5**, 653 (1978).

[17] C. Heller and F.M. Pohl, Nucl. Acids Res. **17**, 5989 (1989).

[18] O.J. Lumpkin and B.H. Zimm, Biopolymers **21**, 2315 (1982).

[19] B.H. Zimm and O. Lumpkin, Macromolecules **26**, 226 (1993).

[20] B.H. Zimm, Polymer Preprints **35**, 173 (1994).

[21] C.R. Calladine, C.M. Collis, H.R. Drew and M.R. Mott, J. Mol. Biol. **221**, 981 (1991).

[22] G.W. Slater and J. Noolandi, Biopolymers **24**, 1781 (1989).

[23] A.G. Ogston, Trans. Faraday Soc. **54**, 1754 (1958).

[24] H.J. Bode, FEBS Lett. **65**, 56 (1976).

[25] M. Zhu, D.L. Hansen, S. Burd and F. Gannon, Journal of Chromatography **480**, 311

(1989).

[26] A.M. Chin and J.C. Colburn, Am. Biotech. Lab., News Edition **7**, 16 (1989).

[27] T. Izumi, M. Yamaguchi, K. Yoneda, T.Isobe, T. Okuyama and T. Shinoda, J. Chromatogr. **652**, 41 (1993).

[28] M. Zhu and S. Hjertén, European Patent Office Publ. No. 0 442 177 A1, 2/13/1990.

[29] D.N. Heiger, A.S. Cohen and B.L. Karger, J. Chromatogr. **516**, 33 (1990).

[30] T. Guszczynski, H. Pulyaeva, D. Tietz, M.M Garner and A. Chrambach, Electrophoresis **14**, 523 (1993).

[31] M. Strege and A. Lagu, Anal. Chem. **63**, 1233 (1991).

[32] P.D. Grossman and D.S. Soane, J. Chromatogr. **559**, 257 (1991).

[33] J.L.Viovy and T. Duke, Electrophoresis **14**, 322 (1993).

[34] K.D. Lukacs, Ph.D. Dissertation, 1983, University of North Carolina, Chapel Hill, NC.

[35] R.L. Bumley, Jr. and L.M. Smith, Nucleic Acids Research **19**, 4121 (1991).

[36] A.S. Cohen, A. Paulus and B.L. Karger, Chromatographia **24**, 15 (1987).

[37] A. Guttman, A.S. Cohen, D.N. Heiger and B.L. Karger, Anal. Chem. **62**, 137 (1990).

[38] J. Liu, V. Dolnik, Y.-Z. Hsieh and M. Novotny, Anal. Chem. **64**, 1328 (1992).

[39] P. Bocek and A. Chrambach, Electrophoresis **13**, 31 (1992).

[40] M. Chiari, M. Nesi, M. Fazio and P.G. Righetti, Electophoresis **13**, 690 (1992).

[41] X.C. Huang, M.A. Quesada and R.A. Mathies, Anal. Chem. **64**, 2149 (1992).

[42] Noolandi, J., Electrophoresis **13**, 394 (1992).

[43] Holmes, D. L., and Stellwagen, N. C., Electrophoresis **12**, 612 (1991).

[44] Stellwagen, N. C., Biopolymers **24**, 2243 (1985).

[45] de Gennes, P. G., *Scaling Concepts in Polymer Physics*, Cornell University Press, Ithaca (1979).

[46] Marciano, Y., and Brochard-Wyart, F., Macromolecules **28**, 985 (1995).

[47] Brochard-Wyart, F., Hervet, H., and Pincus, P., Europhys. Lett. **26**, 511 (1994).

[48] Brochard-Wyart, F., Europhys. Lett. **23**, 105 (1993).

[49] Doi, M., and Edwards, S. F., *The Theory of Polymer Dynamics*, Oxford University Press, New York (1986).

[50] D. Rodbard and A. Chrambach, Proc. Natl. Acad. Sci. USA **4**, 970 (1970).

[51] O. J. Lumpkin, P. Déjardin, and B. H. Zimm, Biopolymers **24**, 1573 (1985).

[52] J. Noolandi, J. Rousseau, G. W. Slater, C. Tumel and M. Lalande, Phys. Rev. Lett. **58**, 2428 (1987).

[53] T. A. J. Duke, A. N. Semenov and J. L. Viovy, Phys. Rev. Lett. **69**, 3260 (1992).

[54] H. A. Lim, G. W. Slater and J. Noolandi, J. Chem. Phys **92**, 709 (1990).

[55] W. D. Volkmuth, T. Duke, M. C. Wu, R. H. Austin and A. Szabo, Phys. Rev. Lett. **72**, 2117 (1994).

[56] G. I. Nixon and G. W. Slater, Phys. Rev. E **50**, 5033 (1994).

[57] F. Brochard-Wyart, Europhys. Lett. **23**, 105 (1993).

[58] E. Arvanitidou and D. Hoagland, Phys. Rev. Lett. **67**, 1464 (1991).

[59] P. Mayer, G.W. Slater and G. Drouin, Appl. Theoret. Electrophoresis **3**, 147 (1993).

[60] M. Doi and S.F. Edwards, Journal of Chemical Society, Faraday Transaction II **74**, 1789 (1978).

[61] M. Doi and S.F. Edwards, Journal of Chemical Society, Faraday Transaction II **74**, 1802 (1978).

[62] M. Doi and S.F. Edwards, Journal of Chemical Society, Faraday Transaction II **74**, 1818 (1978).

[63] M. Doi and S.F. Edwards, Journal of Chemical Society, Faraday Transaction II **75**, 38 (1978).

[64] G.W. Slater, J. Rousseau and J. Noolandi, Biopolymer **26**, 863 (1987).

[65] W. Feller, *Introduction to Probability Theory and its Applications, Vol. 1*, John Willey & Sons, New York (1968).

[66] J.Rousseau, M. Sc. Thesis, 1988, University of Waterloo, Waterloo, On.

[67] G.W. Slater and J. Noolandi, Biopolymers **25**, 431 (1986).

[68] G.W. Slater and J. Noolandi, Macromolecules **19**, 2356 (1986).

[69] B.H. Zimm, J. Chem. Phys. **94**, 2187 (1991).

[70] O.J. Lumpkin, S.D. Levene and B.H. Zimm, Phys. Rev. A **39**, 6557 (1989).

[71] A. Baumgärtner and M. Muthukumar, J. Chem. Phys. **87**, 3082 (1987).

[72] M. Muthukumar and A. Baumgärtner, Macromolecules **22**, 1937 (1989).

[73] G.W. Slater, Electrophoresis 14, 1 (1993).